INVESTIGATING LATERALIZATION OF MOUSE AUDITORY CORTEX USING BILATERAL IN VIVO WIDEFIELD CALCIUM IMAGING

by
Georgia Calhoun

A thesis submitted to Johns Hopkins University in conformity with the requirements for the degree of Master of Science in Engineering.

Baltimore, Maryland
May 2022

Abstract

The survival of most species relies on the ability for individuals to communicate effectively with one another; whether that be during courtship interactions, socialization, or offspring-parent exchanges. In humans, responses to speech are lateralized demonstrating left-hemisphere dominance. Prior studies suggest this lateralization in mice; however, these studies use group averages, which may obscure small differences within one animal that might be observable through examining an individual animal bilaterally. The present study utilizes a novel bilateral in vivo widefield calcium imaging microscope to simultaneously image both hemispheres of awake, head-fixed male and female GCaMP6s transgenic mice. We found that the relative location and topology of auditory cortical areas is highly symmetrical between the hemispheres within individual animals. Vocalizations activate A2, AAF, DM, and UF in both hemispheres. Division of activation between the cortical areas is similar between the hemispheres in response to all stimulus types. However, the left hemisphere shows significantly higher activation in A2 to ultrasonic tones and vocalizations than the right hemisphere. Furthermore, both naïve males and virgin females show a left hemisphere bias in A2 in response to ultrasonic tones and adult vocalizations; however, there is a specific bias in females to pup calls. In conclusion, while topology of auditory cortex is symmetrical across hemispheres, there is a strong left bias in A2 responsiveness to ultrasonic tones and vocalizations.

Thesis Readers

Primary Reader and Advisor: Patrick O. Kanold, Ph.D.

Secondary Reader: Gene Fridman, Ph.D.

Secondary Reader: Web Stayman, Ph.D.

Acknowledgments

I would like to thank my advisor, Patrick Kanold for encouraging me to take on a challenging project and always believing in my abilities. His guidance, along with the genuine and insightful feedback from my peers in the Kanold lab, was crucial to my success on this thesis. Special thanks to Ji Liu for his invaluable perspective throughout multiple stages of the project.

I would also like to thank my partner on the many aspects of this project, Chih-Ting Chen. This project would not have been possible without Chih-Ting, and our partnership in lab allowed us to make incredible progress.

Contents

List of Tables

List of Figures

Chapter 1

Introduction

1.1. Overview

All mammalian species rely on their sensory systems to interpret and interact with the outside world. Sensory systems consist of two main components: cells in the peripheral nervous system that transduce input from the outside world into neural signals and processing centers in the cortex that interpret this information. Because animals rely on sensory processing so extensively, the brain has evolved techniques to make processing sensory information as efficient as possible while also minimizing the energy expended. One way in which efficiency is optimized in the brain is through the specialization of regions to specific tasks. For example, the primary somatosensory cortex (S1), located directly in front of the central sulcus in the parietal lobe, processes a variety of sensations from the skin and inside the body, whereas the primary motor cortex, which is located directly posterior to S1, encodes movement or intent to move[1]. While these two regions neighbor one another, their functionality completely differs. This compartmentalization of tasks allows simultaneous interpretation of sensation of touch stimuli and movement planning, which is essential for many aspects of survival such as hunting, fleeing, or even the execution of dexterous movements.

The brain is composed of two hemispheres connected through a set of pathways known as the corpus collosum. On a large scale, one form of specialization is through the lateralization

of these hemispheres, meaning the hemispheres are designed to handle different tasks from one another. Lateralization between the hemispheres is demonstrated in many systems across the cortex, including the visual and auditory systems. In the auditory system, lateralization has been demonstrated in humans: the left hemisphere is specialized to process speech whereas the right hemisphere primarily encodes spectral information[2]. Delegation of different tasks to the two hemispheres allows for more rapid processing of complex auditory stimuli. Rapid processing is essential because one of the most important aspects of species survival hinges on audition: communication. An important aspect of understanding how the brain processes communicatory sounds is not only establishing how tasks are delegated to different cortical areas, but also determining the underlying circuitry between the hemispheres and how they work together to analyze these complex stimuli. Probing the circuitry of the brain is a complicated feat that sometimes requires invasive measurement techniques; therefore, utilizing animal models such as mice has become common place. Mice are useful in auditory research because many genetics involved in audition have been evolutionarily conserved, and therefore, discoveries in mouse auditory cortex can inform human research[3,4,5]. Mice are also a desirable model because they can be genetically manipulated, which allows for the implementation of useful visualization techniques such as calcium imaging.

1.2. Calcium Imaging

Calcium imaging is a well-established technique to measure and characterize neural activity of mouse cortex in-vivo. When a neuron activates, propagation of an action potential down the axon ultimately depolarizes the membrane along the axon terminal. This depolarization triggers voltage gated calcium channels to open causing a rapid influx of calcium into the cell.

Calcium imaging detects this change in intracellular calcium through the use of calcium-sensitive proteins known as calcium indicators[6]. Calcium indicators are genetically modified proteins that contain a fluorophore that emit fluorescence more strongly when calcium binds. Therefore, an increase in fluorescence indicates increased calcium concentration. In-vivo imaging of cellular processes relies on a particular group of calcium indicators known as genetically encodable calcium indicators (GECIs). GECIs are incorporated into the organisms DNA through transgenes, which allow for expression of the protein of interest through the normal transcription process. GECIs not only allow for a more targeted expression of the calcium indicator into particular cell types, but also a more uniform expression of fluorescence within target cells[7]. In order to visualize activity of excitatory cortical neurons, mouselines are

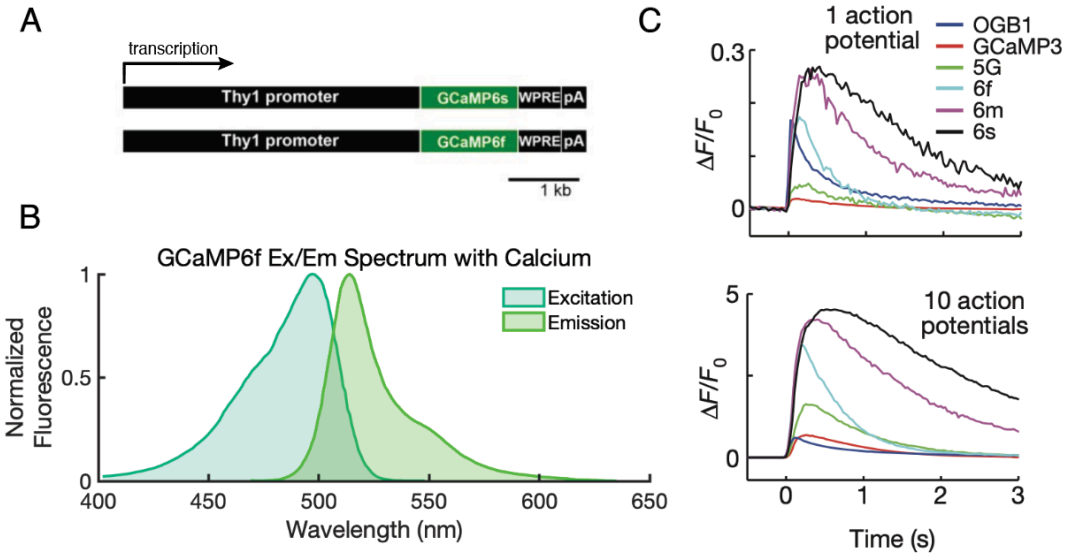

Fig 1.1 *(A)* The insertion of GCaMP6s after the Thy1 promoter allows for expression of the fluorescent protein in all excitatory neurons[8]. *(B)* The excitation and emission wavelengths of the fastest variant of GCaMP: GCaMP6f. GCaMP6f spectrum is similar to that of GCaMP6s with the excitation with calcium bound peaking at 496nm and emission with calcium peaking at 513nm[6]. *(C)* Comparison of the kinetics of different GECIs. GCaMP6s has slower kinetics in comparison, but also creates the largest signal[6].

bred with a transgene that encodes a calcium indicator under the transcription of the Thy-1 promoter[8] (Fig 1.1 A).

A variety of different GECIs exist for different applications that demonstrate different kinetic properties and calcium sensitivities. The most commonly used GECIs for studying mouse cortical activity are GCaMP proteins due to their relatively high sensitivity in comparison to other GECIs. In particular, GCaMP6s has the highest peak change in fluorescence in comparison to other GCaMP variations and is used in the present study despite slower kinetics[6] (Fig 1.1 C).

Calcium imaging has emerged as an appealing alternative to traditional methods, such as measurement of electrical activity through the use of microelectrode arrays, due to the ability to non-invasively and chronically measure neural activity[6]. Calcium imaging has therefore allowed for investigation of cortical activity during development as well as changes in activity before and after training for behavioral tasks. In addition, because neurons are imaged in space, calcium imaging eliminates uncertainty as to what cells or regions correspond to what activity[9]. One limitation of calcium imaging is that it demonstrates lower temporal resolution than electrical measurements because calcium influx has slower kinetics than changes in membrane potential during action potentials[6].

Widefield calcium imaging has proven to be useful in understanding topography as well as to characterize cortical responses. While widefield calcium imaging has lower resolution than microelectrode measurements or 2-photon calcium imaging, this technique allows for visualization of activity over the entire auditory cortex simultaneously. In studying the auditory cortex, widefield calcium imaging has been a useful tool to visualize spatial organization of responses, uncover correlated regions, and locate tonotopic maps.

1.3. Characteristics of Mouse Auditory Cortex

1.3.1 Tonotopic Organization

The topographic organization of mouse auditory cortex has been extensively researched using electrophysiological measurements, widefield calcium imaging, and 2 photon calcium imaging[10,11,12,13,14,15]. From these studies, different interpretations of the organization of mouse auditory cortex exist including divergent findings on gradient direction, division of areas, and tuning properties of fields. In terms of functionality, the function and nomenclature of certain higher order cortical areas is still up for debate (Fig 1.2).

The first mapping of mouse auditory cortex utilized electrophysiological measurements and described five different fields including the anterior auditory field (AAF), the primary auditory cortex (A1), the secondary auditory cortex (A2), the ultrasonic field (UF), and the dorsoposterior field (DP) (Fig 1.2 A). Labeling and characterization of fields, which has been kept relatively consistent across subsequent studies, was adopted from known cortical maps of the cat[16,17]. The results depict AAF and A1, which are considered primary auditory areas, in the center of the auditory cortex with tonotopic gradients pointing in toward one another in the dorsorostral and dorsoventral directions respectively. Areas traditionally regarded as higher order such as A2, UF, and DP were found to surround the primary areas and did not demonstrate tonotopic organization. This mapping showed that A1 and AAF have tonotopic organization in response to tones between 4-40kHz. Tones 40kHz and higher were found to be solely encoded in the UF[10]. A later study also using electrophysiological measurements

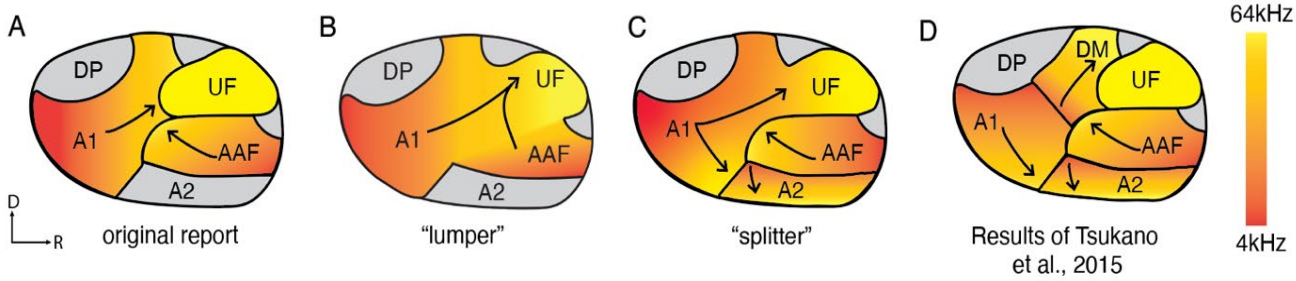

Fig 1.2 *(A)* Original tonotopic map shows A1 and AAF gradients move towards one another, UF is reported as separate area[10]. *(B)* The "lumper" tonotopic map in which UF is a combination of the high frequency regions of A1 and AAF gradients[11]. *(C)* The "splitter" tonotopic map where A1 gradients split in dorsorostral and rostroventral directions[12]. A2 also has gradient moving ventrally. *(D)* More recent schematic of tonotopic organization where A1 gradient moves rostroventrally, and a separate area denoted as DM has gradient moving dorsorostrally[13].

showed similar results; however, UF was determined to be extensions of A1 and AAF rather than a separate area[11] (Fig 1.2 B). In contrast, A2 was found to respond to frequencies across the entire hearing range, with tuning as high as 72kHz[10].

More recent widefield calcium imaging studies pose a different theory of organization in which A1 contains a forked gradient: one gradient moving from low to high frequency in the rostroventral direction whereas the other gradient moves low to high in the dorsorostral direction (Fig 1.2 C). The gradient of AAF was found to move in the caudoventral direction and A2 demonstrated tonotopy in the dorsal to ventral direction[12,14]. Tuning of neurons within each field was investigated with 2 photon imaging and neurons in A1 and AAF were found to have sharper tuning curves with more similar tuning between neighboring cells in comparison to A2[12]. A later study confirmed this organization of gradients, with the distinction that the dorsorostral branch of A1 is instead its own area labeled the dorsomedial field (DM) due to different cytoarchitectural characteristics such as increased number of pyramidal neurons in comparison to other regions within A1[13] (Fig 1.2 D).

Uncertainty exists around not only the tonotopic gradients within these regions but also around the function of these regions. The region of the thalamus that projects to each auditory cortical field can be indicative of the specialized function of that field. The primary auditory cortical areas—A1 and AAF—receive projections from the ventral division of the MGB[17,18,19,20]. Higher order auditory areas are thought to receive projections from non-primary regions of the MGB, such as the dorsal region, as well as from other cortical areas outside of the auditory cortex[17,18,19,20]. A2 has been considered a higher order auditory region in mice because it was found to have similar neuronal properties to A2 in the cat, which is higher order[10,17,21]. Recent literature shows that A2 receives little input from the dorsal division of MGB and instead primarily receives input from ventral division of the MGB[16,18,19,20,22]. However, the pathway from ventral division of the thalamus to A2 is fundamentally different than that of the pathway to A1. In particular, the projections are broader than those to A1, which may explain the broader and more heterogenous tuning of A2 neurons than A1[10,23,24]. Some propose that lack of dorsal projections indicates that what is thought of as A2 in mice is not a higher order area and that categorization of this field as A2 is erroneous. Instead, they propose A2 should be labeled the suprarhinal auditory field (SRAF) in agreement with tonotopic maps defined in rats and that other higher order regions still need to be investigated[15,25]. Therefore, defining higher order regions and describing their functionality is still an active area of research.

1.3.2 Characterization of Vocalization Response

The way in which more complex stimuli such as frequency modulated sweeps and vocalizations are represented within the cortex has also been an active area of research. Mice produce a variety of vocalizations with unique spectral content and timing characteristics depending on the social context. The most common type of vocalization is ultrasonic vocalizations (USV), which are defined as calls that contain frequencies greater than 20kHz and are primarily produced by adult mice, although pups occasionally emit USV's as well[26]. Adult social situations in which USVs are utilized include courtship and mating[26,27], adult male-male interactions, and adult female-female interactions[26,28,29].

Extensive research has been conducted on the types of USV's and the circumstances of their production; however, less research has been carried out on what cortical areas are responsible for processing vocalization stimuli.

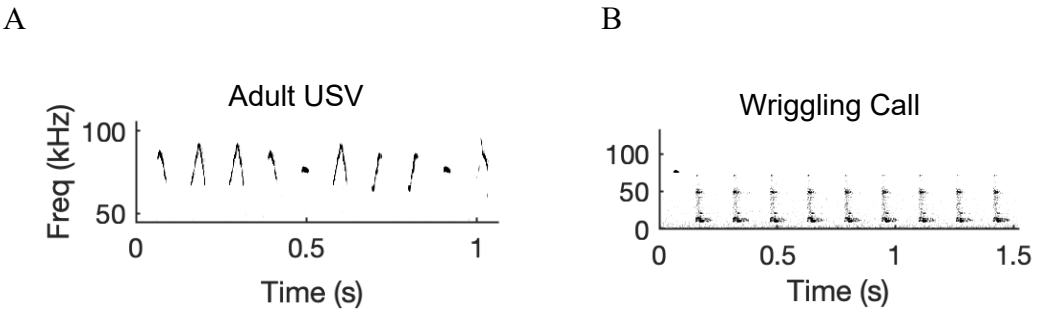

Fig 1.3 *(A)* Example of adult ultrasonic vocalization (USV). Adult USV range between 67-95kHz. *(B)* Shows wriggling call of typical mouse pup. Frequency ranges between 4-80kHz.

Literature investigating cortical areas that respond to adult USV's reveal differing opinions on which areas are most involved. One study found that the dorsomedial field (DM) has a large change in fluorescence in response to courtship vocalizations in females, and this trend

is not shown in males[13]. These findings suggest that salient vocalizations evoke activation of the DM field. Another study suggests that DP and the ventral posterior field (VPAF), which they labeled as the region directly posterior to A2, are the most reasonable options for higher order cortical areas[15]. Other studies find that UF in the right hemisphere has high activation and DP in both hemispheres have low activation to frequency-modulated sweeps similar to those observed in vocalizations, suggesting the involvement of UF and DP in vocalization processing[30]. These findings on cortical regions involved in adult vocalization processing differ; therefore, further investigation is warranted.

Wriggling calls are a common and salient form of communication that correspond to the sounds created when pups attempt to latch onto the mother during nursing[31]. Pup wriggling calls are low frequency around the range of 4kHz and have a similar spectral pattern to human baby crying[32]. One study probed not only what areas respond to the temporal and spectral properties of wriggling calls, but also which areas activate during the recognition process. Using c-Fos immunocytochemistry to label cells responsible for call recognition in female mothers, it was found that call recognition is primarily encoded in A2 and the dorsoposterior field. In addition, dorsoposterior field activity is indicative of responsiveness of the mother[32]. Research on oxytocin and maternal behaviors has shown how the perception of pup calls in the auditory cortex is heavily influenced by the oxytocin system. Oxytocin is a neuropeptide that can lead to neuroplasticity that alters tuning of the entire auditory cortex in mothers[33]. These findings do not reveal particular cortical areas that are most impacted by this neuroplasticity. However, results do show oxytocin impacts the left hemisphere more than the right hemisphere, implying one mechanism by which lateralization may be implemented within mouse auditory cortex[33].

1.4. Lateralization of Auditory Cortex

Human fMRI studies show bilateral activation of the auditory cortex in response to unstructured tones, frequency modulated tones, reversed speech, pseudowords, and words[34]. Imaging studies in human subjects also show functional lateralization of the auditory cortex: left auditory cortex is more involved in temporal processing, while right auditory cortex is more involved in spectral processing[2]. There are reports of bias towards left hemisphere activation in mice in response to different types of vocalizations including courtship vocalizations and pup wriggling calls that parallel the findings in human studies[30,32,35]. Studies using c-fos labeling showed more active neurons labeled in the left hemisphere in response to adult vocalizations than in the right[32,35]. In contrast, the right hemisphere has been found to have higher activation in response to frequencies[30,35]. In terms of structural differences, one electrophysiological study found that the left hemisphere has a larger overall area than the right hemisphere; however, this study did not record both hemispheres within the same mouse and utilized group averages[10,33]. Studies on pup call recognition and mothering behavior show that the left hemisphere has a larger labeled field in A2 than the right hemisphere[32]. In addition, inactivating left hemisphere hinders pup-retrieval in mothers[36]. Lastly, when pup calls with varying inter-syllable intervals (ISI) were presented to experienced females, results showed broader temporal tuning in the left hemisphere, which was shown to improve pup retrieval in comparison to virgins[33]. Evidence of left hemisphere lateralization has been presented using many techniques and contexts; however, comparison of the hemispheres utilizing group averages may obscure individual differences in lateralization. In addition, analysis of activity using c-fos labeling may overlook nuances in the activity that occur in time during presentation

of a stimulus. Bilateral imaging of both hemispheres simultaneously in awake mice has the potential to shed light on these subtleties.

Understanding lateralization between the hemispheres can provide insight into normal functioning as well as auditory processing deficits. For example, structural reorganization causing atypical lateralization of the auditory cortex in children with unilateral cochlear implant may lead to speech processing and sound localization difficulties[37]. Furthermore, abnormal cross-hemisphere communication and lack of lateralization in the auditory cortex is thought to contribute to auditory hallucinations in schizophrenia[38,39]. If lateralization within the mouse auditory cortex is better understood, mice can potentially be used as a model to probe how disruptions in normal lateralization may lead to communication deficits.

1.5. Overview of Present Study

To investigate whether lateralization exists within the mouse auditory cortex, a custom bilateral widefield calcium imaging microscope was used to image both hemispheres of mouse auditory cortex simultaneously. Passive listening experiments were conducted in which transgenic mice expressing GCaMP6s were head-fixed and presented with pure tone and vocalization stimuli.

To test structural lateralization, differences in geometry between cortical areas was visualized and compared between the hemispheres as well as across mice. In addition, area of activation in response to tones and vocalizations was computed and percent of total response area that each activation site occupies was calculated. To test functional lateralization, peak

activation of each cortical area was calculated and compared across the hemispheres. Lastly, response to pup wriggling stimulus was compared between naïve male and virgin female groups to determine sex differences in response to salient vocalization stimuli.

Chapter 2

Microscope Design

We designed and built a bilateral widefield calcium imaging microscope with optogenetic capabilities. Devices were controlled using MATLAB GUI and synchronized using hardware triggering.

2.1 Hardware Design

The widefield imaging setup consists of three main hardware components: 1. the microscope arms to collect imaging data, 2. the laser path for optogenetic stimulation experiments, and 3. the audio system to conduct passive listening experiments (Fig 2.1).

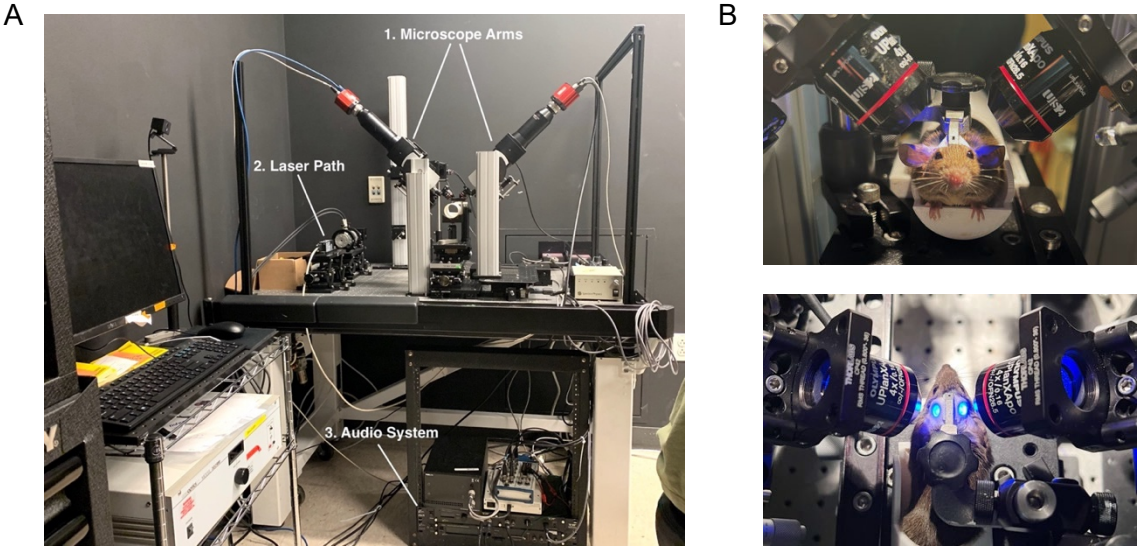

Fig 2.1 *(A)* Image of microscope setup including dual microscope arms, laser path, and audio system. *(B)* Imaging setup with Thy1-GCaMP6s mouse head-fixed under bilateral objectives.

The microscope consists of two rotatable arms to achieve the correct angle to the implanted cranial windows on each side of the cortex. The right arm of the microscope is mounted on a linear stage to allow for easy adjustment of the position of the objective over the cranial window. Each arm contains an adjustable Tube Lens with 0.75x magnification (ThorLabs, WFA4101) that focuses light onto a Scientific CMOS Cameras (Thorlabs, CS235MU) to capture imaging data. The microscope can image transgenic mice expressing jRGECO1a and transgenic mice expressing GCaMP6s; therefore, the imaging light path contains an Olympus filter cube that contains necessary filters and dichroic mirrors (Semrock & Thorlabs, listed in Table 2.1) specific to each fluorescent protein that can be interchanged depending on the transgenic mouse being used. In order to illuminate the cortex, LED's are mounted onto the rotatable arms via magnet to allow the user to easily switch out different wavelength of LED to image different transgenic mice. 470nm LED's (Thorlabs, M470L5) are used to image GCaMP6s transgenic mice and 565nm LED's (Thorlabs, M565L3) are used to image jRGECO1a transgenic mice. The mouse is head-fixed in a custom 3-D printed tube that is fastened to a stage that has adjustability in the X,Y, and Z plane. A sound-insulated housing is built around the imaging components to ensure a quiet environment during passive listening experiments.

In order to conduct optogenetics experiments, the left microscope arm has two lasers in the path: one laser is 473nm (SpectraPhysics, Excelsior Compact CW Laser) chosen to stimulate Channelrhodopsin-2 and the other is 647nm (OBIS 647nm LX) chosen to stimulate ChrimsonR. The desired laser is added into the path using a dichroic mirror (Chroma Technology Corporation). An electro-optic modulator system (Conotopics, M350-80) is used to deliver timed light pulses to the cortex as well as to ensure pulses delivered are of equivalent

power across the entire field of view. The position of the laser light is controlled by an XY galvanometer (ThorLabs, GVS002) that receives input from an NI-DAQ card. An Olympus UPLXAPO 4X Objective is used to focus the laser light and the LED light on the brain. The laser light and the image are focused on the same plane in order to allow for accurate power density measurements of the laser at the plane of stimulation. The LED light is strategically unfocused on the image plane in order to eliminate the possibility of photobleaching or cell death. A schematic of both the imaging and laser light paths are shown in Figure 2.2.

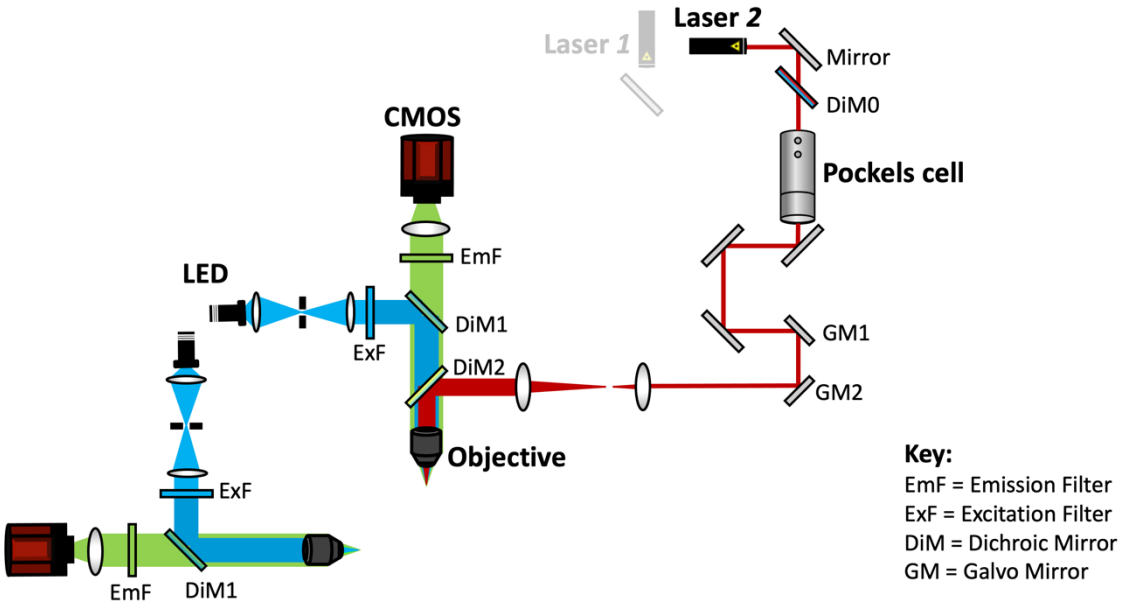

Fig 2.2 Schematic of imaging and stimulation path for GCaMP6s transgenic mice. 647nm laser is guided into path to stimulate ChrimsonR, while 470nm LED is used to excite fluorescence. CMOS camera is used to capture green light emitted from cortex.

	jRGECO1a	GCaMP6s
Laser	**473nm** *(Spectra Physics, Excelsior CW)*	**647nm** *(Coherent, OBIS LX)*
LED	**565nm LED** *(Thorlabs, M565L3)*	**470nm LED** *(Thorlabs, M470L5)*
Emission Filter	**665/150nm** *(Semrock, FF01-665-150-25)*	**535/40nm** *(Chroma Technology Corporation, AT535/40nm)*

Excitation Filter	**550/50nm** *(Chroma Technology Corporation, ET550/50nm)*	**470/40nm** *(Chroma Technology Corporation, ET470/40x)*
Dichroic Mirror 1 (Laser)	**495nm long-pass** *(Chroma Technology Corporation, T495lpxr)*	**550nm short-pass** *(Edmund Optics, 69-215)*
Dichroic Mirror 2 (LED)	**561nm long-pass** *(Semrock, Di02-R561-25x36)*	**499nm FITC** *(Thorlabs, MD499)*

Table 2.1 Summary of optical components used to image both jRGECO1a and GCaMP6s transgenic mice.

In order to perform passive listening experiments, an NI-DAQ board receives software trigger from the computer and sends a synchronized hardware trigger to the cameras, the galvanometer, the Conoptics EO modulator, as well as PA5 and RX6 audio output devices (Tucker-Davis Technologies). PA5 and RX6 audio output devices are connected to a speaker which outputs tone and vocalization stimuli. The synchronized triggering allows for frames captured by the cameras to be aligned with laser stimulation during optogenetic experiments as well as with audio stimuli for passive listening experiments. A diagram of the hardware components is shown in Figure 2.3.

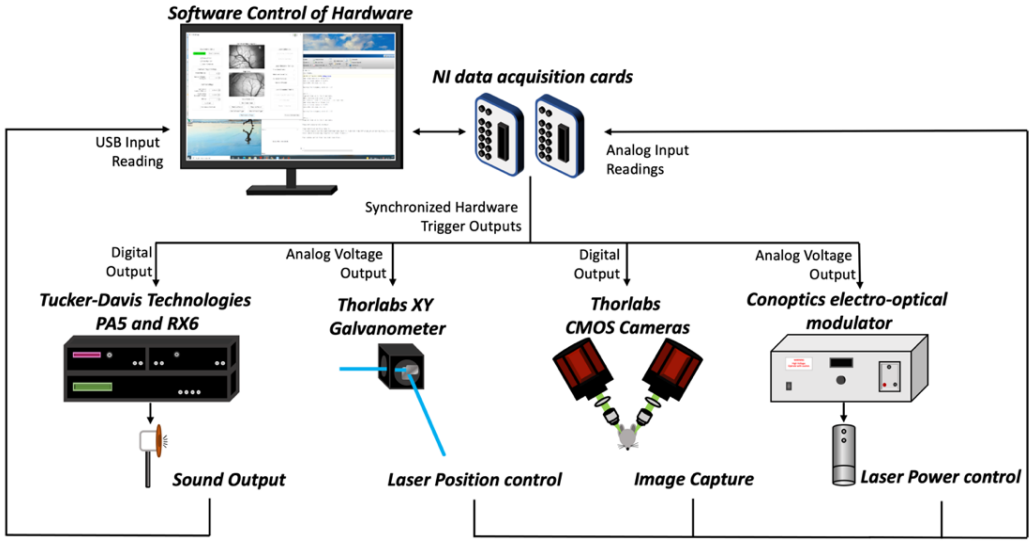

Fig 2.3 Diagram of the control of hardware components. Software signal triggers NI data acquisition cards, which then send appropriate trigger to each component. Devices then send feedback information to computer to ensure proper synchronization.

To ensure that neural activity observed in experiments is independent of brain state, a pupil monitor was built and synchronized to the system to capture the diameter of the mouse pupil throughout experiments. One infrared LED is used to illuminate the mouse pupil, while a second infrared LED is synchronized with the camera acquisition of the microscope arms and flashes in the corner of the image when an image on the microscope is being captured. A third camera (ThorLabs, DCC1545M) is used to capture pupil data.

2.2 Microscope Software

2.2.1 GUI

The hardware components of the microscope are controlled by a custom graphical user interface programmed in MATLAB. The GUI is programmed so that the user can easily input desired settings for frame rate, number of frames to acquire, exposure time, and binning (Figure 2.4).

The GUI contains the following image acquisition options: 1. capturing and saving a single image, 2. a simple software trigger in which the camera is not synched to other devices in the system, 3. a hardware trigger in which the image acquisition will be synched to stimuli, and 4. a live preview option when preparing for imaging. The live preview images can be viewed with a continuously auto-scaled display range—this option is useful when adjusting the LED power and lighting of the image—or the display range of the first image captured—this option is useful when locating areas of activation.

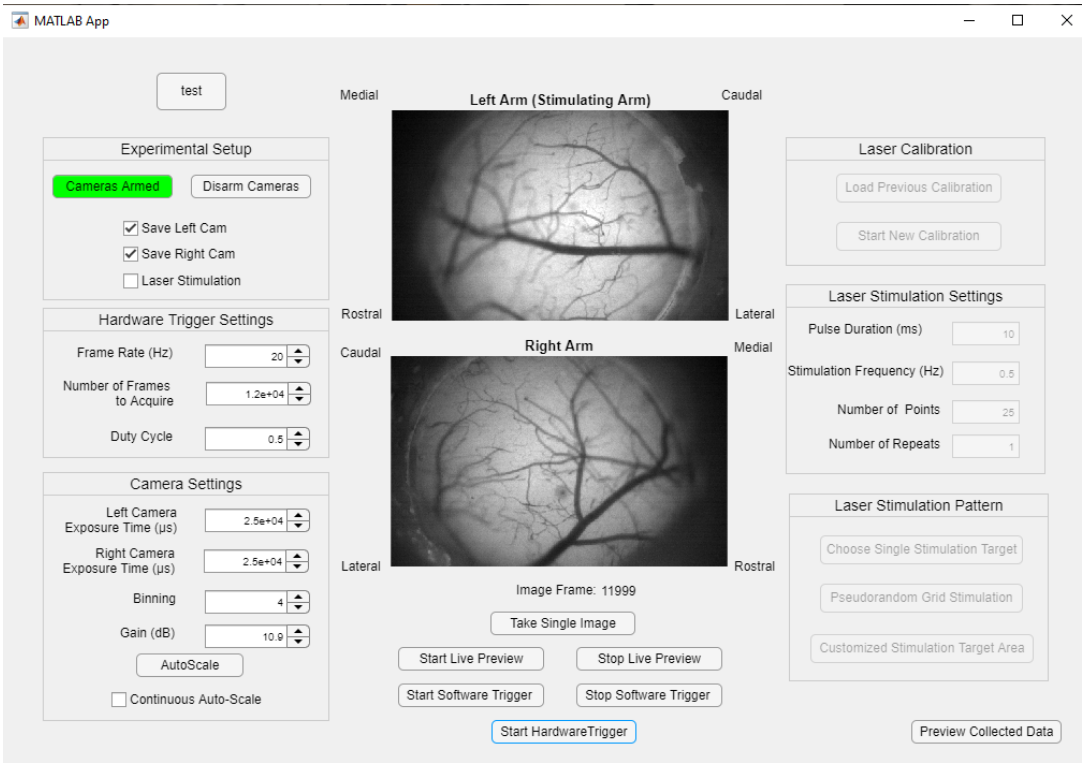

Fig 2.4 The graphical user interface used to control the microscope during experiments. GUI equipped with control of frame rate, exposure duty cycle, exposure time, binning, and gain for CMOS cameras. Customization of laser calibration and pulse control available for stimulation experiments.

If the user wishes to run an optogenetics experiment, they simply check the laser stimulation button and the laser options become available. Before running a stimulation experiment, a calibration of the laser position and power must take place. The user has the option to load calibration data from a previous experiment or to start a new calibration. After calibration, the user can input desired values such as pulse duration of the laser, interphase interval between pulses, number of points to stimulate, and number of repeats of the stimulation pattern. In addition, the GUI has three stimulation pattern choices: the first is the point and click option in which the user chooses a single point in the field of view and the laser will move to the desired position. The next option is the grid stimulation in which

the user chooses a particular number of points within a rectangle they define on the field of view. The laser will then stimulate in a pseudorandom pattern where points are chosen to be maximum distance from one another. Lastly, the user can choose random stimulation, in which the GUI loads previous imaging data with a defined contour around activation areas. The laser will then stimulate in an evenly distributed pattern within the contour.

2.2.2 Laser Calibration

Laser position was controlled by applying an adjustable voltage to the XY Galvanometer. Prior to calibration, voltage applied to the Galvanometer is held at 2.5V for both the X and Y scanning mirrors. Initial laser position is denoted as (x_{CST0}, y_{CST0}) and is in units of pixel location. An initial voltage step of $\begin{bmatrix} V_{1x} \\ V_{1y} \end{bmatrix} = \begin{bmatrix} 0.1V \\ 0.15V \end{bmatrix}$ was applied and the change in position $\begin{bmatrix} \Delta x \\ \Delta y \end{bmatrix} = \begin{bmatrix} x_{CST1} - x_{CST0} \\ y_{CST1} - y_{CST0} \end{bmatrix}$ was determined and the following transfer function was used to relate voltage to laser position: $\begin{bmatrix} V_{2x} \\ V_{2y} \end{bmatrix} = \begin{bmatrix} \frac{\Delta V_x}{\Delta x} & 0 \\ 0 & \frac{\Delta V_y}{\Delta y} \end{bmatrix} * \begin{bmatrix} \delta_x \\ \delta_y \end{bmatrix}$. Using this transfer function, the calculated voltage is applied to the Galvanometer to move the laser to the first point in an evenly spaced 10x10 grid (Figure 2.5 A). The error between the desired location and actual location is calculated and the transfer function is updated according to the following equations:

$$\left(\frac{\Delta V_x}{\Delta x}\right)' = \frac{\Delta V_x}{\Delta x} * \left(1 \pm \frac{Err_x}{pixel_x}\right) * kpx \qquad (1)$$

$$\left(\frac{\Delta Vy}{\Delta y}\right)' = \frac{\Delta V_y}{\Delta y} * \left(1 \pm \frac{Err_y}{pixel_y}\right) * kpy \qquad (2)$$

Err_x and Err_y corresponds to the error in pixel location in the x and y direction respectively calculated with the equation: $x_{CST2} - x_2$ where x_{CST2} is the actual position and x_2 is the desired position. $pixel_x$ and $pixel_y$ corresponds to the total width and height of the image respectively, and kpx and kpy are constants that control how large of a correction step to take. We chose $kpx = 1$ and $kpy = 1$. The

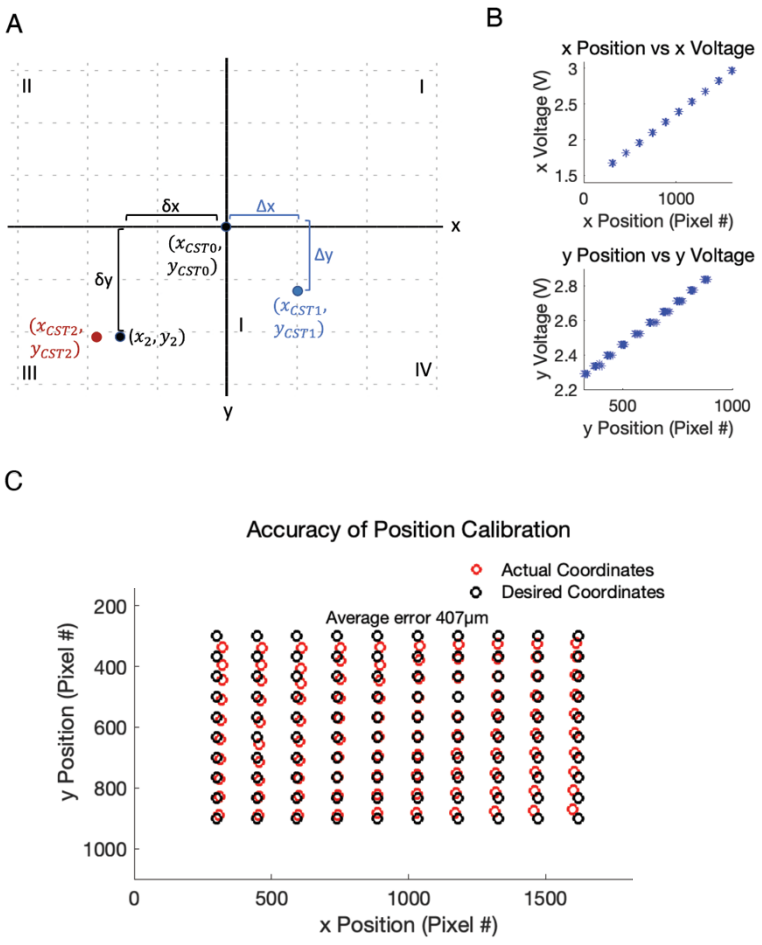

Fig 2.5 *(A)* Initial position of laser shown at origin has pixel coordinates of (x_{CST0}, y_{CST0}). Voltage step used to calculate initial transfer function shown in blue. Desired location of first grid point denoted as (x_2, y_2). Actual position of laser on first step shown in red at coordinates (x_{CST2}, y_{CST2}). *(B)* Relationship between position and voltage in the X and Y direction shown. *(C)* Desired locations in a 10x10 grid shown in black versus actual laser position shown in red. Accuracy drops towards outer edges of field of view.

allowed pixel error was set to be 50 pixels, and this resulted in average accuracy of $16.14\mu m$ in x and $406.98\mu m$ in y with the overall accuracy as $407.30\,\mu m$. Majority of this error results from discrepancy in the y positions in the top left and bottom right corners of the field of view (Fig 2.5 C). The sign in the equation is dependent on the quadrant of the field of view the desired location resides in and the sign of the error. The different possibilities are summarized in Table 2.2. The relationship between position and voltage is linear; therefore, linear regression is used to find the proper voltage to drive the laser to a desired point during stimulation (Figure 2.5 B).

	$Err_x > 0$	$Err_x < 0$	$Err_y > 0$	$Err_y < 0$
Quadrant 1	+	+	-	-
Quadrant 2	-	-	-	-
Quadrant 3	-	-	+	+
Quadrant 4	+	+	+	+

Table 2.2 Summarizes the appropriate sign used in 1 and 2 depending on the quadrant the desired location resides in.

Chapter 3

Methods

Mice were implanted with cranial windows bilaterally. Both hemispheres of mouse auditory cortex were then imaged simultaneously during presentation of pure tone and vocalization stimuli.

3.1 Animals

All procedures were approved by the Johns Hopkins University Animal Care and Use Committee. A total of 8 mice were used: 3 female and 5 male. All mice were imaged between 6-34 weeks of age. For passive imaging experiments, mice with Thy1-GCaMP6s (Jackson Laboratory Stock #024275) were crossed with CBA/CAJ (Jackson Laboratory Stock #000654) to prevent early onset hearing loss. C57BL/6 strain mice are homozygous for the recessive *Cdh23* allele, which causes this hearing loss. The resulting offspring are heterozygous *Ahl*+/*Cdh23,* ensuring they have healthy hearing as well as even expression of GCaMP6s under the promoter Thy1, which is present in all excitatory neurons. All mice were housed in a 12 hour reverse light/dark cycle room.

3.2 Chronic Bilateral Window Implants

Mice were injected with 0.1cc dexamethasone (2mg/ml, VetOne) 2-3 hours before surgery to reduce swelling during surgery. Mice were initially anesthetized with 4% isoflurane (Fluriso, VetOne). Throughout surgery, isoflurane was maintained at 1.5-2.5%. Rectal body

temperature of the mice was maintained at 36ºC using a homeothermic system and a heating pad. Hair on the top of the head was trimmed closely to the skin with scissors; remaining hair was fully removed using Hair Remover Face Cream (Nair). The skin was sterilized by applying Betadine and then 70% ethanol three times. Skin on top of the head was then removed, exposing the skull. Connective tissue was scraped away from the skull using a scalpel in order to prepare the surface for application of the headpost, and the temporal muscle on both sides was resected to create space for two cranial window implants. Cyanoacrylate (Vetbond) was applied to open incisions to prevent bleeding and infection. Removing excess temporal muscle from both sides may result in difficulty chewing and disrupt ability to eat; therefore, great care was taken to leave rostral muscle intact on both sides. The headpost was then secured to the top of the head using both super glue (Loctite) and dental acrylic (C&B Metabond, Parkell). A craniotomy with a diameter of approximately 3mm was performed over the left auditory cortex first and the opening was cleaned and prepared for cranial window implant. The cranial window consisted of two circular 3mm glass coverslips and one circular 4mm glass coverslip secured together using optic glue (NOA71-Norland Products). Silicone elastomer (Kwik-Sil, World Precision Instruments) was carefully placed around the edge of the 4mm coverslip and the window was implanted with 3mm coverslips facing towards the cortex. Dental acrylic was carefully applied around the 4mm coverslip to further secure the window in place. The same process was then repeated on the right side of the skull: anatomical landmarks such as the temporal ridge, lambdoid suture, and the medial cerebral artery were used to ensure window symmetry across hemispheres. Immediately following surgery, mice were injected with 0.1cc Dexamethasone, 0.05cc Cefazolin (1g/vial, West Ward Pharmaceuticals), and 5mg/kg of Carpofen (0.5mg/mL, Zoetis US) and placed under a heat lamp for 30 minutes for recovery.

For three days following surgery mice were injected with 0.1cc Dexamethasone and appropriate Carpofen dose once a day to ensure proper healing from surgery. In addition, antibiotic water (Sulfamethoxazole and Trimethoprim Oral Suspension, USP 200mg/40mg per 5ml, Aurobindo Pharms USA; 6ml solution diluted in 100ml water) replaced normal drinking water for 7 days following the procedure.

3.3 Auditory Stimuli

Mice were presented with pure tones in the typical mouse hearing range, pure tones in the ultrasonic range, and vocalizations. Pure tones were generated using MATLAB scripts obtained from Liu et al., 2019[14]. The peak amplitude of the tones was calibrated to 70dB SPL using a Brüel & Kjœr 49440A microphone (Fig 3.1 C). Tones in the typical mouse hearing range used were between 4kHz to 64kHz with logarithmic spacing and 2 tones per octave, meaning a total of 9 frequency levels were played. A total of 5 ultrasonic tones were played between 70kHz to 94kHz with an even spacing of 6kHz. 9 different vocalization stimuli were created using the "virtual mouse organ"[29], in which syllables recorded from mice were combined into bouts using a third order Markov Model. Each bout fell between 64kHz to 94kHz and contained 10 syllables. Vocalizations of p100 mice and older were used (Fig 3.1 A). Vocalization stimuli were fed through a whitening filter from 4kHz-95kHz and calibrated so that the average of the peak sound level was equivalent to 70dB (Fig 3.1 B). Both sound and vocalization stimuli were played for 1 second with a 3-3.5 second pause of silence in between. Each tone and vocalization stimulus was played at 35dB, 50dB, 65dB. Stimuli were

played in a random order to prevent prediction of stimulus. For both tones and vocalizations, each stimulus was repeated 10 times.

Bilateral response to pup wriggling calls was investigated by playing a stimulus consisting of a bout of 10 wriggling calls totaling to 1.5 seconds with 3-3.5 seconds of silence in between. Each stimulus was repeated 10 times at 35dB, 50dB, and 65dB. Pup vocalization stimuli were calibrated using the same method as adult vocalization stimuli (Fig 3.1 A).

Sound waveforms were loaded into a RX6 multi-function processor (Tucker-Davis Technologies) and fed through a PA5 attenuator (Tucker-Davis Technologies) to output the

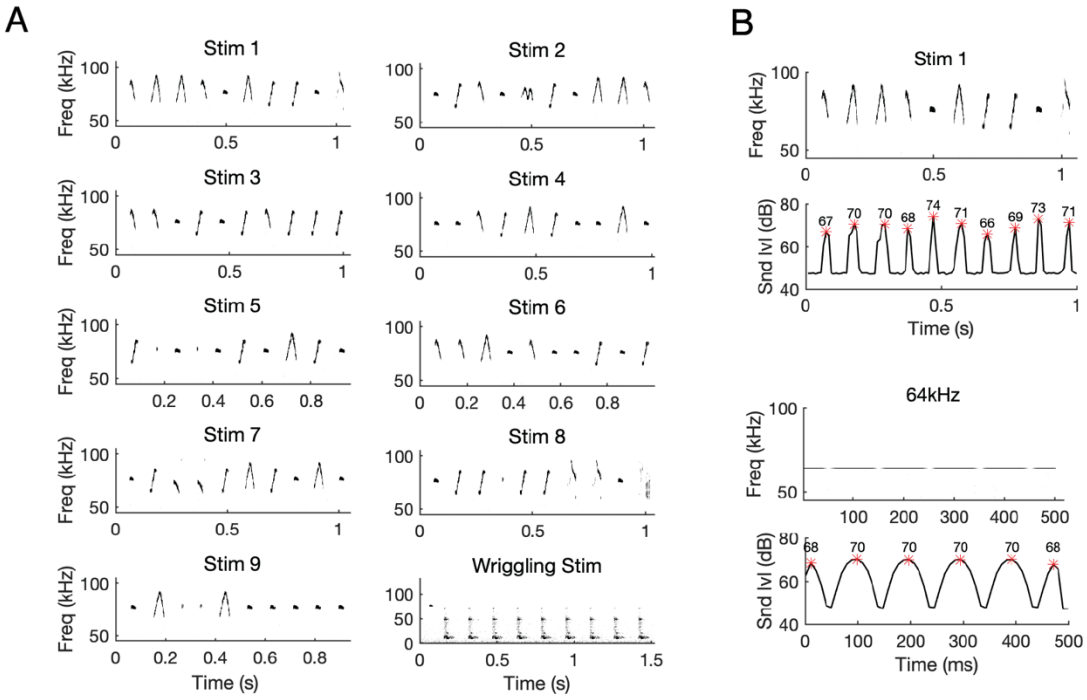

Fig 3.1 *(A)* Stimulus 1-9 show spectral content of adult vocalization stimuli used. Each stimulus contains 10 syllables between 67-95kHz and last 1 second long. Stimulus 10 shows the pup wriggling call which contains frequencies between 4-64kHz and lasts 1.5 seconds. *(B)* Calibration techniques used for vocalization stimuli (top) versus tone stimuli (bottom). Peak of all syllables averaged to 70dB for vocalizations. For tones, once peak of sinusoid reaches 70dB, calibration is complete.

intended sound level. Output from the PA5 was fed to a ED1 speaker driver and subsequently a ES1 electrostatic speaker (Tucker-Davis Technologies). Because auditory stimuli presented to one ear preferentially activates the contralateral hemisphere and since we intended to image neural activity in both hemispheres, the speaker was placed directly in front of the mouse at a distance of 10cm to prevent bias in activity of one hemisphere. In total, tone and vocalization experiments lasted ~67 minutes.

3.4 Widefield Imaging

Mice were placed inside a custom plastic tube and head-fixed in place using a custom Aluminum headpost and headpost holder (Shapeways). The bilateral widefield microscope (description in section 2.1) was equipped with two 470nm LED (Thorlabs, M470L5), Excitation Filter (Chroma Technology Corporation, ET470/40x), FITC dichroic mirror (Thorlabs, MD499) Emission Filter (Chroma Technology Corporation, AT535/40m) for excitation of GCaMP6s fluorescent protein. Image acquisition was controlled through the custom GUI (description in section 2.2). Images were captured at a frame rate of 20Hz with a 25ms exposure time and 4x4 binning. LED power was controlled using an external voltage source, which ensured constant and equivalent LED power in both imaging paths. LED power was fixed between a range of 2.9-3.1mW for all experiments.

3.5 Image Processing

3.5.1 Image Pre-Processing

Images were motion corrected using MATLAB functions "imregconfig" to find the optimizer and metric for a monomodal image followed by "imregtform" using a translational geometric transformation as well as the optimizer and metric from "imregconfig." The outer 10 pixels on all sides of the motion corrected images were then cropped out, which was found to improve ROI detection. Motion corrected images were downsampled by a factor of 2 using MATLAB function "imresize", resulting in an image of dimensions 141x231. For each stimulus, the mean of the 4 frames prior to the playout of the stimulus was used as the baseline fluorescence level for that stimulus. The dF/F of the 20 frames corresponding to the playout of the stimulus was calculated for each of the 10 repeats. Then the mean of the 20 playout frames was taken and the mean over the 10 repeat trials was calculated, resulting in a single image, referred to as the activation image, which summarizes the activation in response to each stimulus (Figure 3.2).

3.5.2 Determining total Area of Activation

The area of activation to each stimulus was calculated by averaging the activation images across all attenuation levels (35dB, 50dB, 65dB) then applying a gaussian filter using "imgaussfilt" with sigma 1.5 to the averaged image to eliminate noise (Fig 3.2). Singular value decomposition was performed on the gaussian filtered images and the first 10 principal components were used. The images were binarized using "imbinarize" at two different thresholds: one threshold at 50% of the maximum value in the image and one threshold at

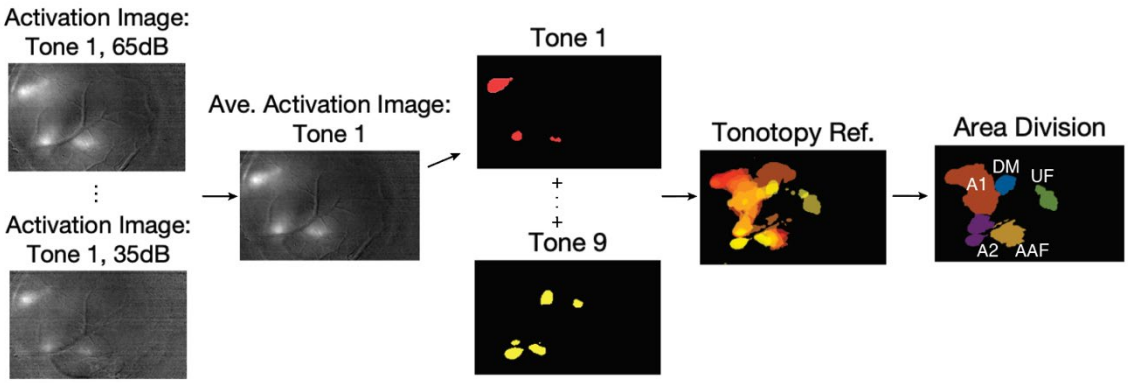

Fig 3.2 Activation images for each stimulus are averaged across all sound levels then resulting image is pre-processed then thresholded. 50% of maximum value threshold is shown above. Active area to each stimulus are summed and pixel responsive to any one stimulus is considered active. Division of area is determined from tonotopic gradients manually.

35% of the maximum value. The binarized images for each stimulus were summed together, and any pixel > 1 was considered active. The number of pixels within the binarized images were calculated using the "bwarea" function. The number of pixels was multiplied by a conversion factor in order to find the area in μm. A 0.01mm stage calibration slide (MUHWA) was used to find that the length of one pixel in an image without binning corresponds to 1.86μm. The conversion factor was calculated using the following equation:

$$\frac{(d * b * 1.86\mu m)^2}{(1 * 10^{-6})\mu m^2/mm^2} = CF$$

Where d corresponds to the downsampling factor (2) and b corresponds to the binning factor (4). The conversion factor was calculated to be $2.21 * 10^{-4} \frac{\mu m^2}{pixel}$. Division of auditory cortex into subregions was achieved by overlaying tonotopic gradients to manually trace which regions of the binarized image correspond to what cortical areas (Fig 3.2). Percent of total area is calculated as follows:

$$\frac{area\ of\ subdivision}{total\ voc.\ area} = \%\ of\ voc.area\ ,\ \frac{area\ of\ subdivision}{total\ tone\ area} = \%\ of\ tone\ area.$$

Percent of total active area responsive to tones and vocalizations was compared across hemispheres and across mice and corrected paired sample t-tests were used to determine differences in distribution of activation across hemispheres.

3.5.3 Determining Peaks of Activation

Peaks of activation are determined in similar fashion to section 3.5.2; however, no averaging across attenuation level or stimuli are done prior to thresholding. A gaussian filter with sigma 1.5 was applied to the activation images corresponding to each stimulus. Singular value decomposition was performed on the gaussian filtered images and the first 10 principal components were used. The images were binarized using "imbinarize" with threshold set to

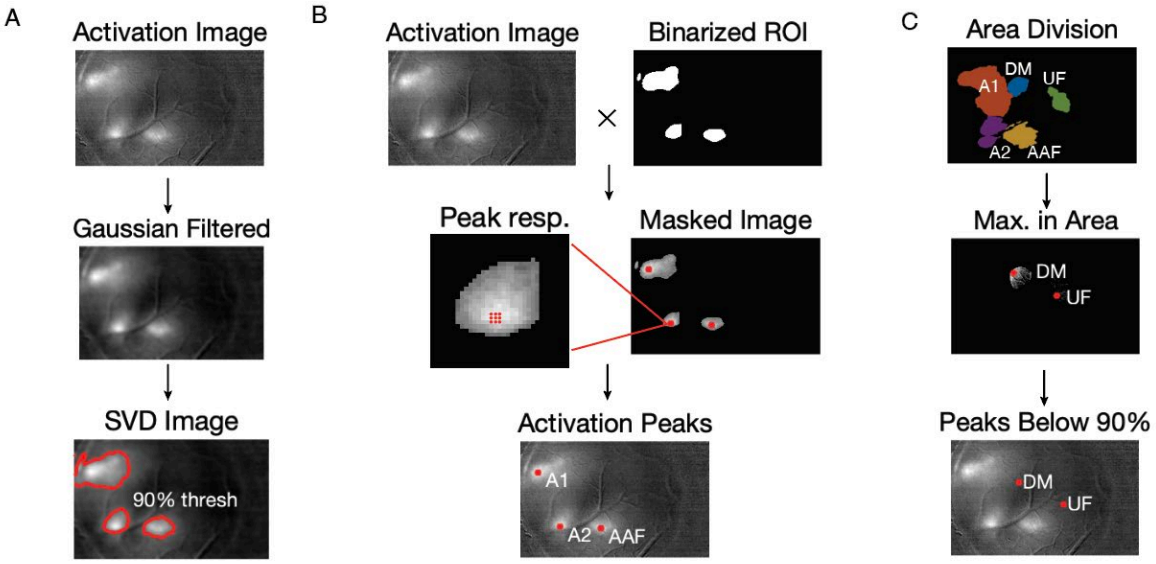

Fig 3.3 *(A)* Activation image for each stimulus is gaussian filtered and singular value decomposition is performed. Images are binarized using 90th percentile threshold. *(B)* Mask is applied to original activation image and active regions are labeled with proper cortical area. Average of 3x3 square surrounding maximum value of each cortical area is calculated. *(C)* For cortical areas that do not reach 90th percentile, maximum 3x3 square within the total area for that region is calculated.

pixels within the top 90th percentile, resulting in a mask of the active areas. The ROI mask was overlayed over the original activation image to isolate the active regions. Each area of activation was assigned to a particular cortical area A1, A2, AAF, DM, or UF using the tonotopic gradients as reference (Figure 3.3 B). The peak fluorescence response within each area was then calculated by finding the maximum pixel value within the ROI and then taking the average of a 3x3 pixel square around the maximum pixel. Accuracy of each peak location was confirmed by manually ensuring location fell on cortex rather than blood vessel or window edges. Only activity falling within the top 90th percentile was considered a peak for geometric comparisons. For comparison of activation strength of each cortical area, if activity within a particular cortical area did not fall within the top 90th percentile, a 3x3 square around maximum pixel value of the total area of that region based on tonotopic gradients was used (Fig 3.3 C). Peak activation of each area was compared across left and right hemispheres. Peak activation values were compared across animals and trials and paired-sample t-tests were used to determine significant differences between the left and right hemisphere.

3.5.4 Calculating geometry between cortical areas

Geometry between cortical areas was calculated using a global coordinate system with the barrel cortex set as origin. To locate the barrel cortex, ten minutes of spontaneous activity was collected. Data was motion corrected and dF/F was calculated. Baseline fluorescence was calculated using a moving window of 27.5 seconds to correct for drift in fluorescence throughout the experiment. Left and right hemisphere images were stitched together and pixels located within the cranial windows were isolated. Pixel-wise correlation was calculated

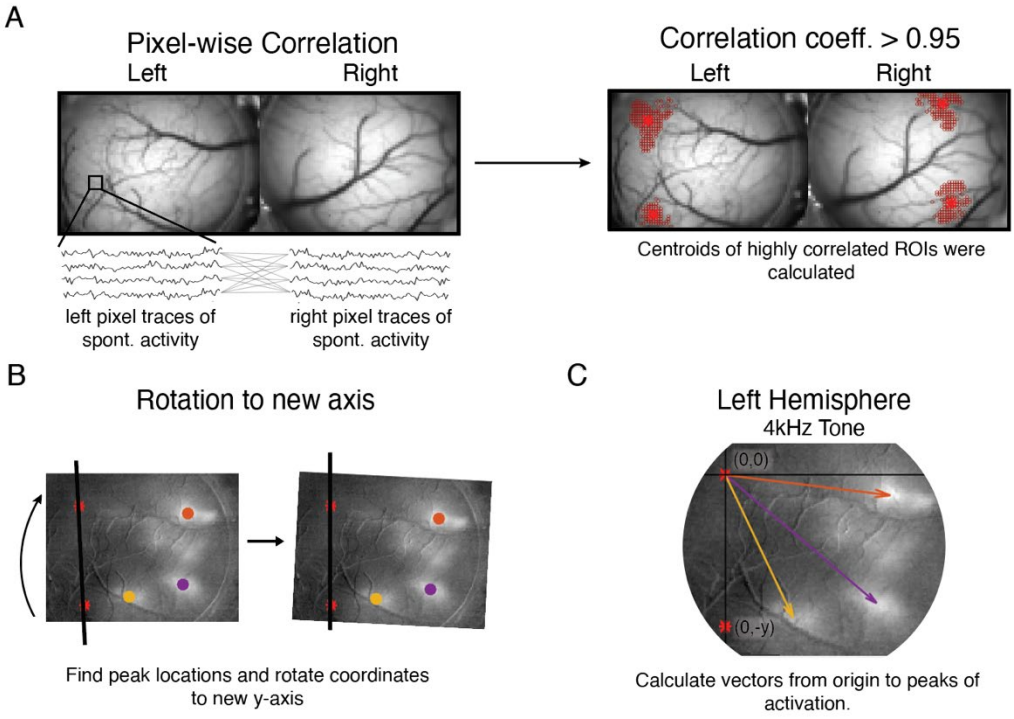

Fig 3.4 *(A)* Pixel-wise correlation was used to identify symmetrical and highly correlated ROIs. Centroid of hotspots with correlation coefficient > 0.95 was calculated. *(B)* Dorsal centroid is set as origin (0,0) and rostral ROI is as y-intercept. A line between the points was calculated and rotated to be vertical. All coordinates were rotated to this new vertical axis. *(C)* Vectors between origin and each location of peak activation was determined.

using MATLAB function "corrcoef" (Figure 3.4 A). Contralateral correlation was visualized by restricting the correlation distance to 500 pixels. Pixels that had correlation coefficient of 0.95 were found to be located in the barrel cortex which contained two hotspots: one located dorsal to the auditory cortex and one located rostral to the auditory cortex (Figure 3.4 A). The centroids of each hotspot were calculated for both hemispheres by taking the average pixel locations within a particular hotspot. Then, the dorsal centroid and rostral centroid were used to create the y-axis of a global coordinated system and the coordinate system of the images were rotated accordingly (Figure 3.4 B)

Peak locations for each attenuation and stimulus were determined using the method in section 3.5.3. Peak locations for each stimulus were averaged over all attenuation levels. Coordinates for 4kHz and 5.7kHz were averaged together to represent the low tone peak activation location. Coordinates for 16kHz and 22.6kHz were averaged together to represent the mid tone peak activation location, and 45.3kHz and 64kHz were averaged together to represent the high tone peak activation location. Vectors between the new origin and each peak location (with coordinates rotated to the new axis) were determined (Figure 3.4 C). Right hemisphere axes were rotated around the y-axis, aligned, and overlayed onto the left hemisphere axes to visualize differences between left and right hemisphere locations (Fig 3.2. B). The total distance between peak locations in left and right hemisphere were calculated and compared across different cortical areas and frequency levels.

Chapter 4

Results

Within each individual mouse, spatial organization of responses and magnitude of activation across both hemispheres were analyzed.

4.1 Activation Patterns in Response to Tones and Vocalizations are Similar Across Hemispheres

In order to investigate similarities and differences in cortical activity across the hemispheres in response to tones and vocalizations, we performed bilateral widefield imaging on awake, head-fixed CBA/CaJ x Thy1-GCaMP6s mice (n = 5 naïve male and n = 3 virgin female) ranging from 6 weeks – 24 weeks in age. Mice were chronically implanted with windows bilaterally using the lambdoid suture and temporal ridge as references, which allowed us to achieve similar field of view across the hemispheres (Fig 4.1 A,C).

First, we set off to characterize the response to tone and vocalization stimuli in both hemispheres. We observed topography that aligns with prior results: two tonotopic gradients move towards one another in the dorsorostral and dorsoventral directions corresponding to A1 and AAF respectively[10,12,14] (Fig 4.1 B,C). A2 sits most ventrally and shows a dorsoventral gradient. We found that A1 responds to tones ranging from 4-95kHz at 65dB, which is 20khz higher than the previously reported range[10] (Fig 4.1 D). We found gradients in A2 and AAF

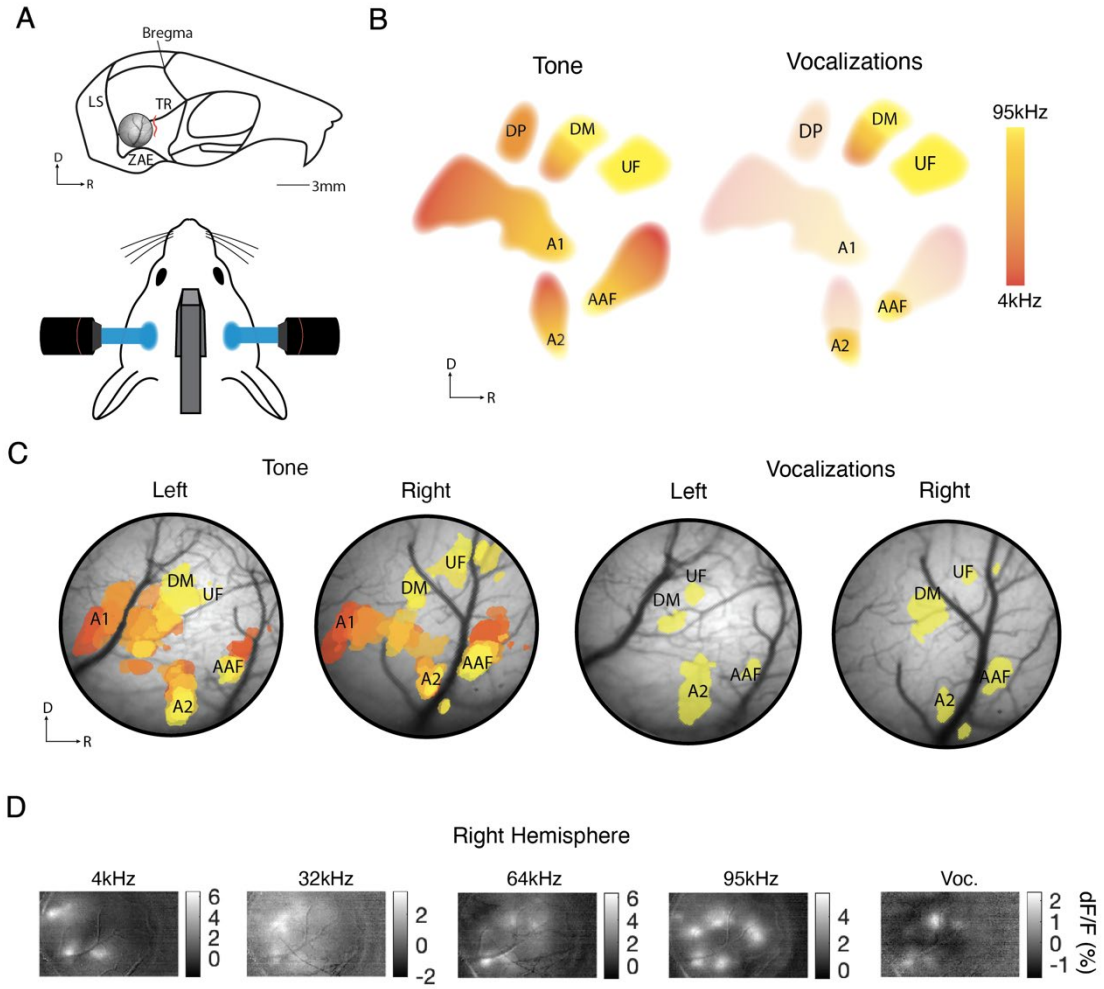

Fig 4.1 *(A)* Anatomical landmarks on skull used for bilateral window implant (LS = lambdoid suture, TR = temporal ridge, ZAE = zygomatic arch extension). Schematic of bilateral imaging setup: speaker placed 10cm directly in front while awake mouse is head-fixed from behind. *(B)* General diagram across all mice of response to tones and vocalizations. Vocalizations activate high frequency regions of cortical areas. *(C)* Tonotopic map and vocalization response in exemplar mouse using 95% threshold to determine ROIs. Topography of tone and vocalization response is highly similar between the hemispheres. *(D)* Activation hot-spots are shown in right hemisphere. 95kHz tone activates all cortical areas at 65dB, vocalizations activate high frequency regions of A2, AAF, DM, UF, with little activation in high frequency region of A1.

also reach up to 95kHz at 65dB. We identified another tonotopic gradient tuned to frequencies 40kHz and higher moving dorsorostrally from A1, which we denoted as the dorsomedial field (DM)[13]. The DM sits adjacent to the ultrasonic field (UF), which is also tuned to high frequencies, but shows no gradient[10,11,12,13]. These tonotopic gradients appear highly similar in both hemispheres (Fig. 4.1 C). Adult ultrasonic vocalizations primarily activate the high

frequency regions of A2, AAF, DM, and UF in both hemispheres, with little to no activation in the high frequency region of A1 (Fig 4.1 B,C,D). Similar to tones, activation patterns in response to vocalizations show little difference between the hemispheres.

Overall, both tones and vocalizations demonstrate very similar activation patterns in both hemispheres. In addition, there is no vocalization specific region, rather vocalization stimuli activate the same cortical areas as tones apart from decreased activation in A1.

4.2 Locations of Peak Activation are Highly Symmetrical Across Hemispheres

The symmetricity between the hemispheres was probed more quantitatively by projecting locations of peak activation within the auditory cortex to a global coordinate system and comparing these peak locations across hemispheres (Fig 4.2 A). We found that two ROIs with correlation greater than 95% exist in the most dorsal and rostral poles of each cranial window. These ROIs are highly symmetrical across the hemispheres and consistent across mice, which makes them desirable reference points for a global coordinate system (Fig 3.4 A). Visually, geometry of peak locations at each frequency showed little variation between the hemispheres within individual mice as well as across mice. When compared quantitatively, the peak locations between the hemispheres were highly similar: average difference between left and right hemispheres within an individual mouse across all frequencies and cortical areas is 154.0μm (std: 92.4μm) (Fig 4.2 C).

Next, we compared whether topography is more similar within an individual than across the group. The average difference in peak location across all mice was 304.1μm (std: 168.3μm)

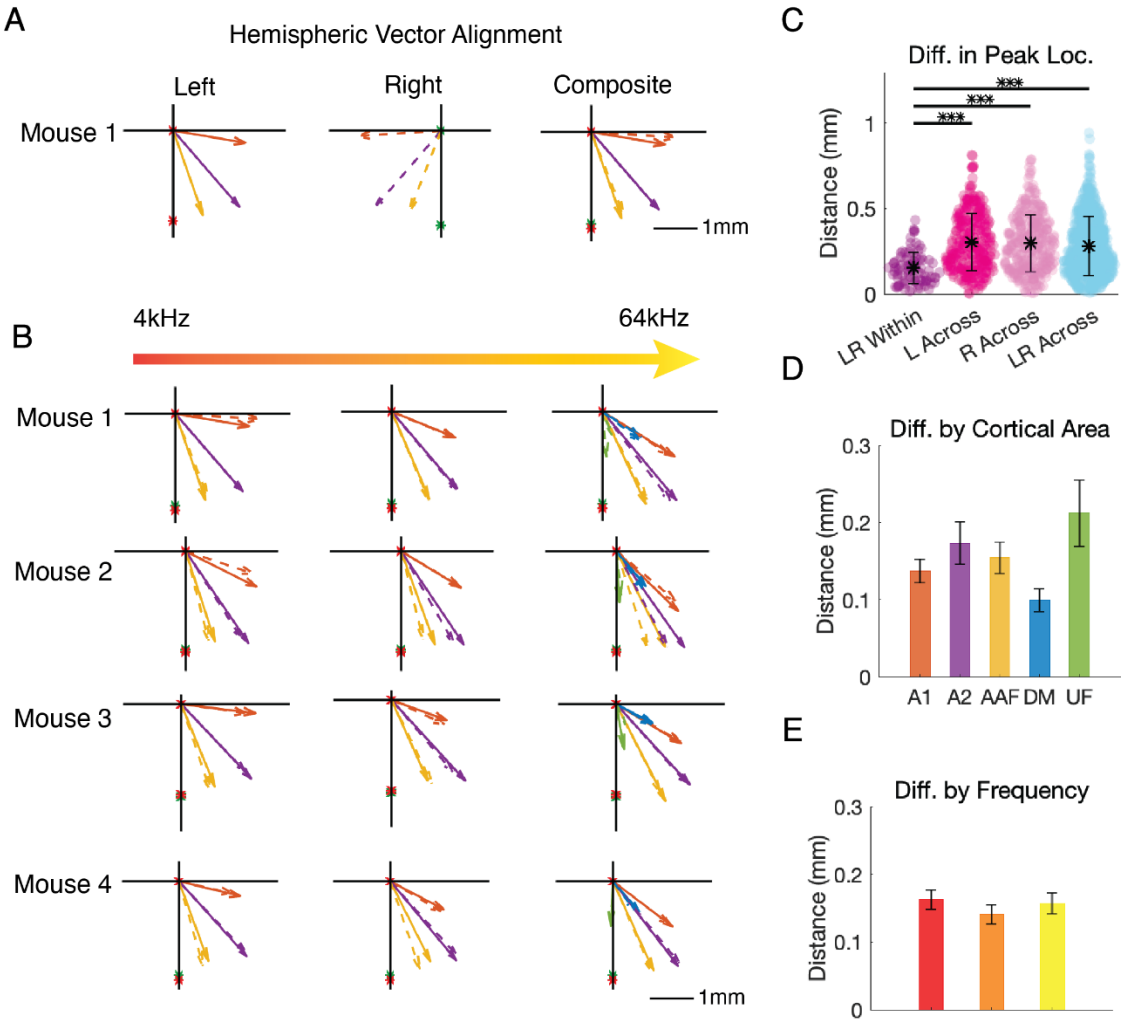

Fig 4.2 *(A)* Left and right coordinate planes are overlayed to visualize differences in peak locations across hemispheres for example mouse 1. Left hemisphere depicted as solid lines, Right hemisphere depicted with dashed. *(B)* Geometry of 4 example mice across low (4kHz-5kHz), mid (11kHz-16kHz), and high (40kHz-64kHz) frequencies. *(C)* Difference between left and right peak locations within individual mice versus across mice. *(D)* Difference in location within a particular cortical area. *(E)* Difference in location depending on frequency of stimulus.

for the left hemisphere and 298.6μm (std: 165.4μm) for the right hemisphere (Fig 4.2 C). Comparing left versus right hemispheres across mice results in a difference of 282.4μm (std: 171.2μm). For all cases, difference in peak location across mice is significantly higher than differences within individuals (L across: $p < 8.7e^{-15}$, R across: $p < 2.89e^{-14}$, LR across:

$p < 7.73e^{-12}$). While individual differences are often expected across animals, our findings show that across mice, the locations of cortical areas only differ by approximately 0.3mm, which is relatively small considering how differences in experience can impact cortical organization. However, topographic organization is still more similar within an individual animal, which highlights the need for bilateral analysis when doing cross-hemisphere comparisons.

We observed a small trend for the distance between peak locations across hemispheres and the cortical area in which the peak location falls (Fig 4.2 D). Peaks located in DM (distance: 99.2μm) show the lowest difference across hemispheres as well as the lowest variability across mice (std: 41.3μ), whereas peaks in UF (distance: 212.1μm, std: 121.0μm) and A2 (distance: 172.9μm, std: 78.5μm) show the highest distance and standard deviation. However, differences between cortical areas are not significant and this should be investigated further with larger population size. Lastly, the relationship between frequency of the stimulus and the difference in peak activation across the hemispheres was investigated and no trend was observed (Fig 4.2 E). Our results indicate that topography between the hemispheres within an individual mouse is symmetrical regardless of stimulus frequency. However, not all cortical areas have the same uniformity between hemispheres. A2 and UF have the largest difference in location between the hemispheres, which could indicate some form of hemisphere-specific specialization in those areas and should be tested further.

4.3 Vocalizations Preferentially Activate A2

While location of peak activation was revealed to be symmetrical, another way in which cortical organization may differ between the hemispheres is in the total area of activation in response to different stimuli. Evidence has shown that the left hemisphere has larger cortical area[10] and that more neurons in the left hemisphere are activated in response to vocalizations than in the right hemisphere[32]. Larger number of recruited neurons may lead to both higher magnitude of response as well as a higher activation area. In order to better understand how the area of activation in each hemisphere may differ in response to tone and vocalization stimuli, adult male (n = 5) and female mice (n = 3) were presented with 4-95kHz tone stimuli and adult ultrasonic vocalization stimuli ranging from 70-95kHz. Tone stimuli were divided into two groups: hearing range frequencies (4-64kHz) and ultrasonic frequencies (70-95kHz) to better parse whether differences in activation are due solely to spectral content or due to more complex characteristics of the stimuli. First, we calculated the total area of activation in response to a stimulus type, then the percent of total area for each cortical area was determined based on tonotopic gradients and compared (Fig 4.3. A). For male and females grouped together, total activation area in response to hearing range tones is approximately twice as large as ultrasonic tones and three times as large as vocalizations in both hemispheres for both threshold cut-offs (Fig 4.3. B). Right hemisphere shows a higher activation area than left hemisphere for all three stimulus categories; however, this difference is only significant for ultrasonic tone stimuli ($p = 6.63e^{-0.4}$ for 35% and $p = 0.0049$ for 50%) (Fig 4.3 B). In looking at sex differences, male and females have nearly identical area of activation for ultrasonic tones and vocalizations; however, males have slightly higher area of activation in response to hearing

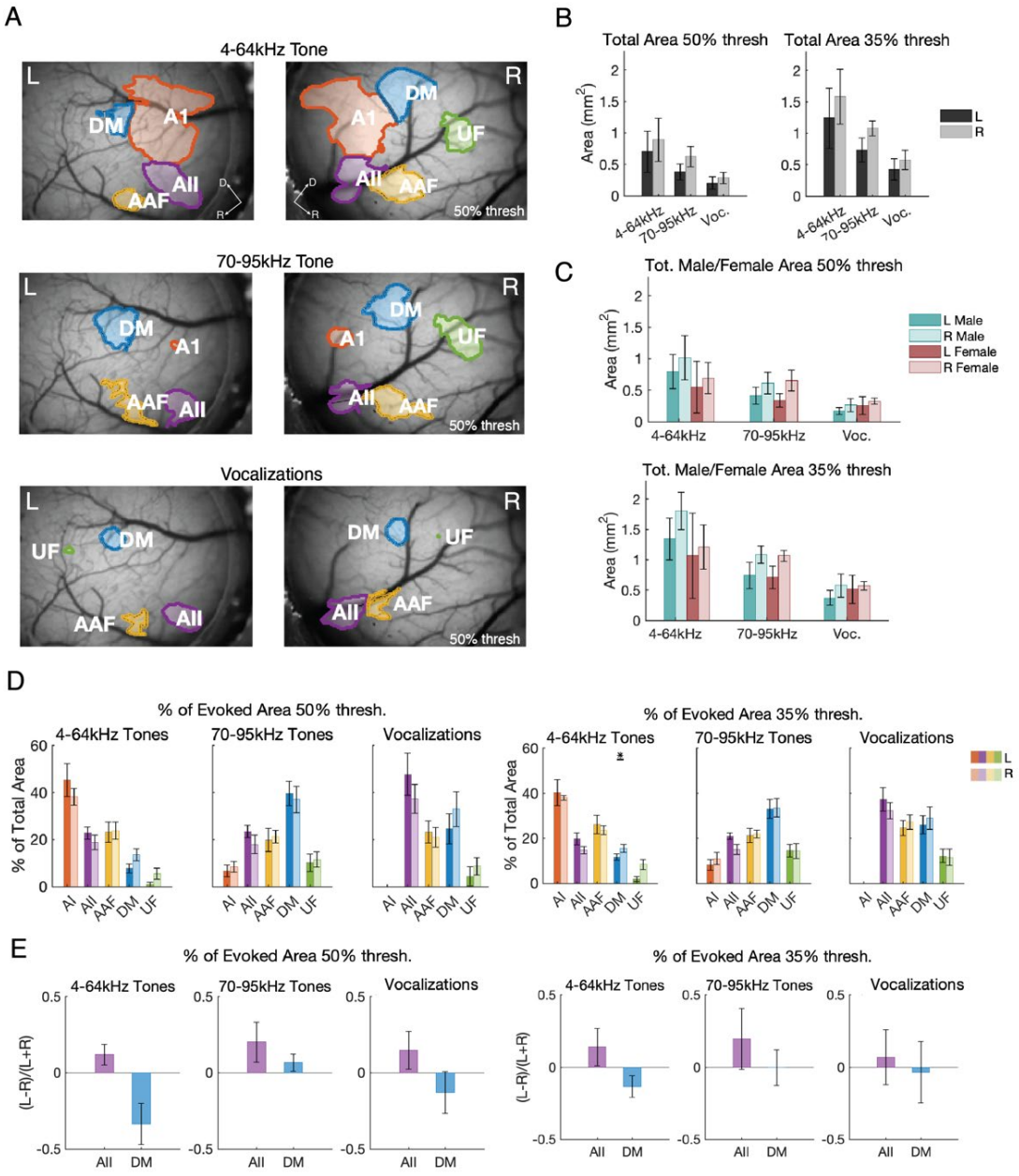

Fig 4.3 *(A)* Images illustrating area of activation for each cortical area across all stimulus types. High frequency tones and vocalizations evoke smaller area of activation across all cortical areas. Vocalizations evoke little to no activation in A1. *(B)* Total area of activation in response to each stimulus type at 50% max. and 35% max. thresholds. *(C)* Comparison of male versus female total area of activation to each stimulus type. *(D)* Percent of total area each cortical area occupies in the left and right hemisphere. Allocation of cortical areas changes depending on the stimulus type. *(E)* Bias ratio of A2 and DM in response to each stimulus type. A2 shows slight left hemisphere preference to all stimuli, whereas DM shows slight right hemisphere preference to 4-64kHz tones and vocalizations.

range tones for each hemisphere although this is not significant. Overall, no significant differences between total area in left and right were observed for neither male nor female

groups, which differs from previous findings that the left hemisphere has higher overall area than right hemisphere[10].

Division of activation between the cortical areas was dominated by A1 for hearing-range tone stimuli for both thresholds in both hemispheres (Fig 4.3D). For ultrasonic range tones, percent of total area allocated to A1 drastically drops, and instead DM takes up a higher percent of the total area in both hemispheres (Fig 4.3D). In response to vocalizations, percent area dedicated to A1 drops to 0%, and instead A2 dominates. However, the division of activation across cortical areas in response to vocalizations is highly variable across mice. The average trend shows that in the left hemisphere at 50% threshold, A2 occupies 47.8% (std = 25.4%) of total area whereas AAF occupies 23.2% (std = 13.1%), DM occupies 24.5% (std = 18.0%), and UF occupies 4.3% (std = 11.2%). In the right hemisphere at 50% threshold, A2 occupies 37.3% (std = 17.5%) of total area whereas AAF occupies 21.0% (11.5%), DM occupies 33.0% (21.0%) and UF occupies 8.7% (10.7%). This trend is also observed at the 35% threshold cut off (left A2 = 37.5% (std = 14.8%), left AAF = 24.5% (std = 9.4%), left DM = 25.9% (std = 11.3%), left UF = 12.14% (std = 8.3%); right A2 = 32.2% (std = 10.0%), right AAF = 27.2% (std = 9.0%), right DM = 29.04% (std = 14.3%), right UF = 11.48% (std = 10.5%)) (Fig 4.3D).

When comparing percent of total area a cortical region occupies in the left versus right hemisphere, DM showed significantly higher percent of total area in the right hemisphere at 35% threshold (R = 15.4%, L = 11.68%, p = 0.0084) (Fig 4.3D). However, no other difference between the hemispheres is observed for low frequency tones or high frequency tones. In response to vocalizations, left hemisphere A2 appears to take up slightly higher percentage than right, while right hemisphere DM appears to take up slightly higher percentage than left;

however, these findings are not significant ($p > 0.05$). To see whether differences between left and right hemisphere may be minimized due to averaging across the mice, we also looked at the ratio (L-R)/(L+R) for A2 and DM (Fig 4.3 E). However, we found very high variability across mice and no clear trend of hemispheric dominance for either A2 or DM to any of the stimulus types. These findings suggest that the hemispheres do not significantly differ in the way in which the activity is divided across the cortical regions.

In summary, no difference between breakdown of activation area into cortical regions was observed between the hemispheres. In addition, we observed high variability across mice when looking at the ratio of percent of total area between left and right. While no differences between the hemispheres was found, we did notice that in both hemispheres, A2 occupies a larger portion of the total area than all other cortical areas in response to vocalizations; however, high variability exists across animals and this should be investigated further.

4.3 Vocalizations Evoke Higher Response Amplitude in A2

We had two objectives in measuring peak response: the first was to confirm findings on what cortical areas have the strongest response to vocalizations, and the second was to determine whether the strength of response differed between the hemispheres. Prior studies have proposed functional lateralization of the auditory cortex in mice in which the left hemisphere specializes in vocalizations, and the right hemisphere is more tuned to slow frequency modulated sweeps[30,35]. In order to better understand how both hemispheres work together to process tone and vocalization stimuli, adult male and female mice were presented

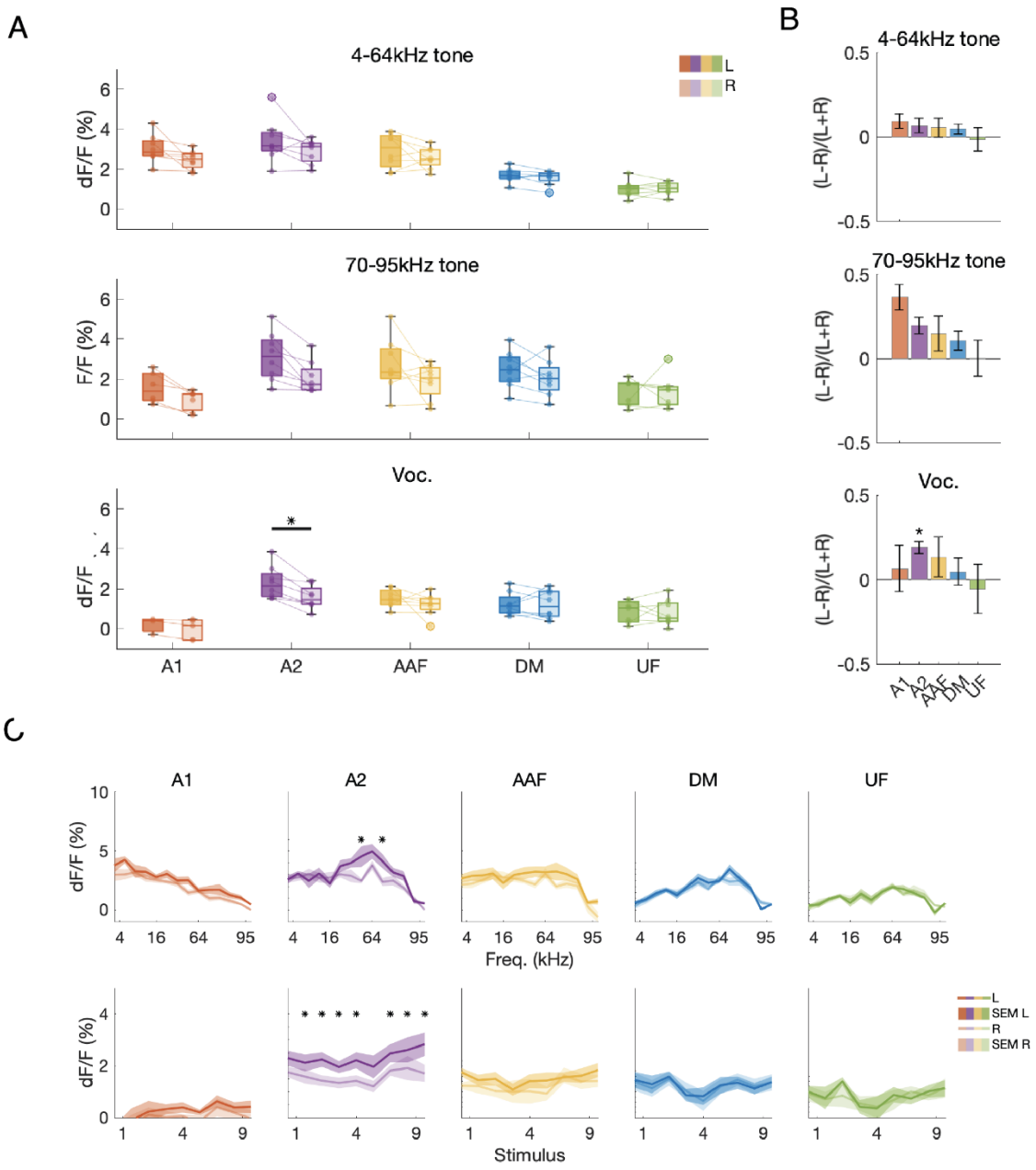

Fig 4.4 *(A)* Comparison of dF/F between the hemispheres across all trials of each stimulus category. All animals show higher activation of left hemisphere in response to vocalizations in A2. *(B)* The ratio (L-R)/(L+R) is compared for each cortical area. Preference to left hemisphere in A2 occurs in response to vocalizations. *(C)* dF/F of each mouse is averaged and plotted across tone stimuli and vocalization stimuli. Left hemisphere A2 has higher response than all other cortical areas. Left hemisphere bias in A2 is apparent in tones between 40-80kHz as well as seven out of 9 vocalization stimuli.

with 4-95kHz tone stimuli and adult ultrasonic vocalization stimuli ranging from 70-95kHz. For every mouse, peak activation of each cortical area across all trials of a particular stimulus were averaged together and plotted (Fig 4.4. B). Each line connects the left hemisphere and

right hemisphere response within one animal. We found that a left hemisphere bias exists in response to 70-95kHz tones ($p = 0.0063$) and vocalization stimuli ($p = 0.0023$). For vocalization stimuli, all 8 animals demonstrated this left hemisphere bias. In addition, the left hemisphere A2 shows higher activation than all other cortical areas regardless of hemisphere. No other cortical areas show a significant hemispheric bias. While previous literature has proposed that DM is important to vocalization processing, we did not find significantly higher activation or hemispheric bias in this area[13]. When looking at the ratio:

$$(left\ activation - right\ activation)/(left\ activation + right\ activation)$$

we see that for tones a very small bias to the left hemisphere for all cortical areas aside from UF (A1 = 0.094, A2 = 0.068, AAF = 0.056, DM = 0.047, UF = -0.014). In response to both 70-95kHz tones and vocalizations, the preference to left hemisphere of A2 increases to 0.197 ($p = 0.11$) and 0.192 ($p = 0.0089$) respectively.

Because A2 shows a left hemisphere bias to both 70-95kHz tones and vocalization calls, we investigated how peak activation changes as a function of tone frequency. When plotting peak activation averaged across mice versus the stimulus presented, A2 begins to show a left hemisphere bias in response to high frequency tones 32kHz-82kHz in addition to vocalization stimuli (Fig 4.4 A). No other cortical areas show significant difference between hemispheres to tones at any frequency nor vocalizations. Left hemisphere bias in A2 is once again confirmed across each of the stimuli, with seven out of the nine vocalization stimuli evoking significantly stronger response in left A2 in comparison to right A2 ($p < 0.05$). These results support the notion that left hemisphere is more selective to vocalization stimuli due to higher responsiveness to frequencies within the vocalization range; however, it is inconclusive from these findings whether A2 is involved in any higher-order functioning specific to vocalization

processing. Utilization of more targeted stimuli or experiments to silence A2 signaling may help to clarify these uncertainties.

4.4 Wriggling Calls Evoke Higher Response Amplitude in A2 for Virgin Females

One important vocalization is the wriggling call evoked by pups attempting to latch to mothers for suckling[27,31]. Recognizing pup calls is a critical function of female mice and is reliant on the oxytocin system as well as encoded in the auditory cortex[33]. Oxytocin is a neuropeptide that is known to contribute to maternal behavior as well as cortical plasticity. Oxytocin activation leads to cortical plasticity in the auditory system that enhances pup call recognition and improves in pup retrieval behavior[33]. One way in which oxytocin influences the auditory cortex is through broadening the tuning to inter-syllable intervals (ISI). Findings show that this tuning is lateralized: left hemisphere has broader temporal tuning than right hemisphere to calls with varying ISIs mimicking pup distress calls[33]. While experienced females showed more robust responses to a variety of pup calls, virgin females showed equal responsiveness to prototypical pup calls[33]. Another experiment investigating auditory cortical response to pup calls used c-Fos immunocytochemistry and showed cells responding to wriggling call recognition reside in A2 and that the left hemisphere has a larger labeled field than the right hemisphere[32]. In addition, inactivating left hemisphere hinders pup-retrieval in mothers[36]. Previous experiments evaluating pup retrieval behavior in virgin females co-housed with pups shows that the oxytocin system is activated by co-housing. While auditory tuning

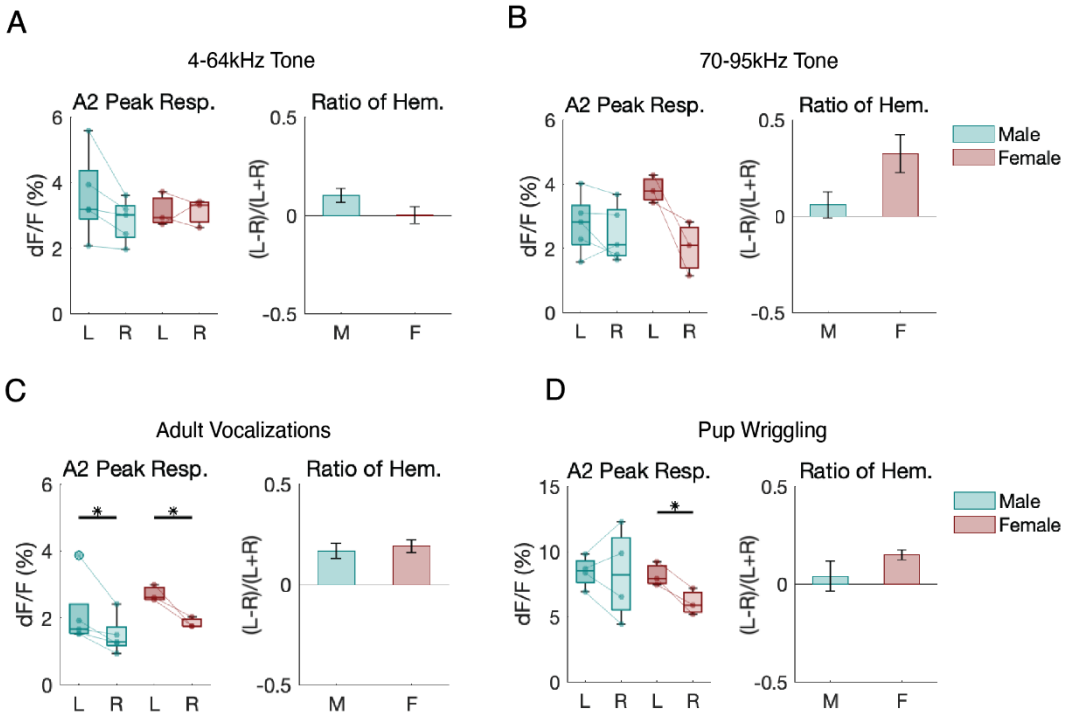

Fig 4.5 *(A)* Peak response in A2 of males versus females in response to 4-64kHz tone. Neither group shows a significant difference between the hemispheres. *(B)* Peak response in A2 of males versus females in response to 70-95kHz tones. Females begin to show a left hemisphere bias that is not significant. *(C)* Peak response in A2 of males versus females in response to adult vocalizations. Left hemisphere response is significantly higher in both male and female with a near equivalent bias ratio. *(D)* Peak response in A2 of males versus females in response to pup wriggling call. Only females show significant left-hemisphere bias.

and maternal behaviors are improved with oxytocin activation due to exposure to pups, we wanted to investigate whether a left-hemisphere bias in females existed prior to this process.

In the present study, we compared responsiveness of naïve male and virgin female mice. We tested whether A2 showed higher responsiveness to pup wriggling calls and whether this response was lateralized. We also investigated whether there was a sex-dependent difference in activation to tones, adult vocalizations, and pup calls. We found no significant difference between the magnitude of male and female responses to 4-64kHz pure tones and no lateralization for either sex was present (Fig 4.5 A). In response to 70-95kHz pure tones, females begin to show a left hemisphere bias with a bias ratio of 0.325 (std = 0.210) however, this difference is not significant ($p = 0.099$) (Fig 3.4.B). Both male and female groups show

slightly significant left bias lateralization to adult vocalizations ($p = 0.0496$, $p = 0.0496$) with similar ratio of left bias (male = 0.1670, std = 0.0857; female = 0.1906, std = 0.0706) (3.4.C). In response to pup wriggling calls, the magnitude of both male and female responses increases substantially (4.5 D). Male responses increase from an average of 2.10% (left) and 1.47% (right) for adult vocalizations to 8.43% (left) and 8.28% (right) for pup wriggling. Female responses increase from 2.71% (left) to 1.84% (right) to 8.19% (left) and 6.08% (right) (4.5 C, D). Although both sexes show increased responsiveness, only females show significant left hemisphere lateralization with a bias ratio of 0.19 (std = 0.071). No other cortical areas show lateralization in response to pup wriggling calls. These findings confirm that A2 activation increases in response to pup wriggling calls and that there is lateralization towards the left hemisphere observed solely in virgin females in response to these pup calls.

Chapter 5

Discussion

Imaging both auditory cortices simultaneously revealed both the similarities and differences in how each of the hemispheres are structured and the way in which they function. We found that the general activation pattern to tones and vocalizations is highly symmetrical across the hemispheres. Because topography of the auditory cortex is proven to be experience driven, higher similarity between the hemispheres within an individual is expected. However, following this same line of thinking, individual differences across animals are also expected due to differences in experience. Our results confirm that both qualitatively and quantitatively the locations of peak activation are highly similar within an individual animal. However, we found that even across mice, the difference in peak location was still less than 0.3mm, which suggests that the development of gradient size, position, and direction is relatively uniform across different animals. Next steps could be to probe whether presenting different stimuli to different ears within an individual animal or presenting different stimuli to different animal groups during development increases the difference in peak location across hemispheres and across animals. These experiments could help determine to what extent the relative position of peak activation is influenced by experience and whether the symmetricity between hemispheres and the similarities in positioning across mice can be disrupted.

Similar to location of cortical areas, the percent of total area dedicated to each cortical area also shows no significant differences across the hemispheres. In terms of total area of activation, our findings show that the right hemisphere had a larger total area of activation than left hemisphere; however, this finding is not significant. Neither of these findings exactly align with prior results which have shown a significantly larger area and number of neurons recruited in left hemisphere auditory cortex. However, our findings may be explained by the method in which area of activation was computed. Percentile thresholds-- in which a pixel is considered active if it is within the top 95^{th} percentile of pixel values-- cannot be used to calculate total area of activation because this will result in the same number of pixels being outputted. Therefore, we used a threshold that is some percentage of the maximum pixel value. When using this method, activation that has a high peak of activation but drops off more rapidly will appear as a smaller area, whereas activation that is a lower peak and has a more gradual drop off will appear as a larger area of activation. Perhaps activation across the right hemisphere has a lower peak and more gradual decrease in fluorescence, which would explain the discrepancy to prior literature. Further analysis on whether differences in the shape of activation between the hemispheres exists and is impacting these calculations needs to be conducted. Using a threshold that is some percentage of the maximum value may also explain the high variability across animals because there may be large differences in the shape of the peak across animals.

While our results suggest no differences in area of activation between the hemispheres, our findings on percent of total area dedicated to each cortical areas within a hemisphere are useful. These findings show that in response to lower frequency tones A1 is primarily activated, in response to high frequency tones DM is primarily activated, and in response to vocalizations

A2 is primarily activated. The high percentage of area dedicated to A2 in response to vocalizations may indicate that A2 is involved in processing of these more complex stimuli and parallels our findings on the amplitude of response.

In response to vocalizations, no unique areas activate, rather the high frequency regions within the tonotopic map respond. However, highest activation occurs in A2 in both hemispheres, and A2 in the left hemisphere has significantly higher amplitude of activation than right A2. These findings suggest that A2 is involved in vocalization processing in some capacity; however, the mechanism by which this is occurring is yet to be confirmed. In just analyzing USVs, no conclusion could be made about whether the left hemisphere just allocates more resources to processing of high frequency tones, or whether A2 is involved in the processing of higher-level stimuli. Because we see this left-hemisphere bias for vocalization stimuli that contain lower frequencies at a high power such as in the wriggling call (Fig 4.5), this suggests that not only is left A2 more attuned to high frequencies, but it also is involved in some higher-level aspect of processing of vocalization stimuli that are salient to the listener. Future directions using this novel bilateral microscope include optogenetic experiments to either enhance or inhibit left hemisphere A2 in response to different types of vocalizations in order to test the impact this has on behavior. These types of experiments are necessary to confirm the exact function of A2 in processing more vocalization stimuli.

We found left-hemisphere bias in virgin females in response to pup calls; however, we were unable to investigate this effect in mothers. Bilateral imaging on mothers in response to pup calls should be conducted to compare whether the left-hemisphere bias in A2 to pup calls is enhanced in mothers, and whether disruption of this pathway specifically disrupts pup retrieval behavior. While it has been shown that inactivation of the entire left auditory cortex inhibits

pup retrieval behavior in mothers[36], specifically knocking out activity in A2 could help focus what particular region within left auditory cortex is necessary for maternal behaviors. It has also been shown that oxytocin plays a large role in maternal behaviors and also significantly impacts plasticity and tuning in left auditory cortex[33]. Experiments probing whether oxytocin impacts A2 tuning and activation could be useful to further understand the mechanism that allows mothers to recognize pup calls and act accordingly.

Our findings in A2 align nicely with experiments investigating cross-hemisphere correlation using this same microscope setup[40]. Noise correlations between ROIs during tone presentation as well as during spontaneous activity were calculated (Fig 5.1). High noise correlations indicate that signaling within two areas vary together. Therefore, high noise correlations suggest high connectivity between two regions. The results show that cross-hemisphere correlations between A2 are significantly lower than all other cortical areas, implying lower cross-hemisphere connectivity in A2. Higher connectivity between the hemispheres could indicate higher similarity in functioning since both hemispheres are sharing the same information, whereas lower connectivity could indicate lower similarity in functioning between the hemispheres since less information is shared. The lower connectivity in A2 may signify that there is some hemisphere-specific specialization occurring in A2 that is not occurring in the other cortical areas.

The specialization to each hemisphere to different tasks may present itself in different ways within the auditory cortex: location of activity, the area allocated to a certain function, as well as the level of activity dedicated to a particular stimulus type. Through the use of a bilateral calcium imaging microscope to image both hemispheres of awake mice simultaneously, we were able to more accurately identify the distinctions between the auditory cortex within each

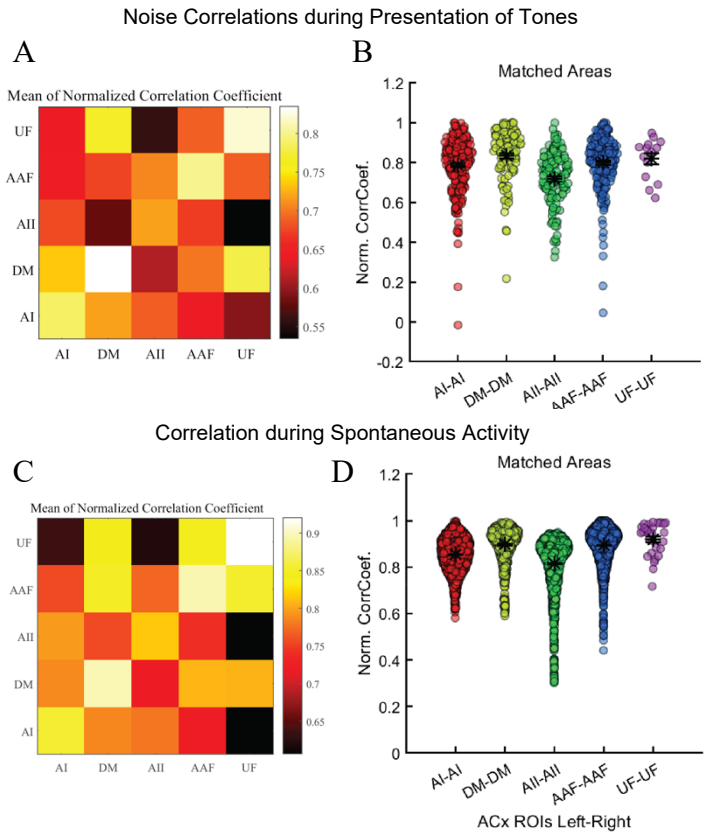

Fig 5.1 *(A)* Noise correlations are calculated between cortical areas across hemispheres during tone experiment. Heat map shows normalized correlation coefficient. Looking along the diagonal, left and right A2 show lower correlation than other cortical areas. *(B)* Shows the normalized correlation coefficients of each ROI across all mice. Left and Right A2 again show significantly less correlation. *(C)* Correlation of spontaneous activity during experiment where no auditory stimulus is played. Left and right A2 again shows lowest correlation in comparison to other cortical areas. *(D)* Normalized correlation coefficient between each ROI across all animals is plotted and again shows lower correlation of A2[40].

hemisphere. We found that location of cortical areas is highly symmetrical. The percent of total area A2 occupies in response to vocalizations points towards A2 as a prominent cortical area for vocalizations processing. In addition, the higher activation amplitude in left hemisphere A2 in response to adult and pup vocalizations further confirms prior findings that mice demonstrate left-biased lateralization within the auditory cortex. Moving forward, this new technique of bilateral widefield calcium imaging can be used to pinpoint the exact circuitry underlying this lateralization we have observed to better understand mammalian speech processing and communication.

References

1. Borich, M. R., Brodie, S. M., Gray, W. A., Ionta, S. & Boyd, L. A. Understanding the role of the primary somatosensory cortex: Opportunities for rehabilitation. *Neuropsychologia* **79**, 246-255 (2015).

2. Zatorre, R. J. & Belin, P. Spectral and Temporal Processing in Human Auditory Cortex. *Cerebral cortex (New York, N.Y. 1991)* **11**, 946-953 (2001).

3. Ehret, G. & Riecke, S. Mice and Humans Perceive Multiharmonic Communication Sounds in the Same Way. *Proceedings of the National Academy of Sciences - PNAS* **99**, 479-482 (2002).

4. Ohlemiller, K. K. Mouse methods and models for studies in hearing. *The Journal of the Acoustical Society of America* **146**, 3668-3680 (2019).

5. Vandamme, T. F. Use of rodents as models of human diseases. *Journal of Pharmacy & Bioallied Sciences* **6**, 2-9 (2014).

6. CHEN, T. *et al.* Ultrasensitive fluorescent proteins for imaging neuronal activity. *Nature (London)* **499**, 295-300 (2013).

7. Afshar Saber, W., Gasparoli, F. M., Dirks, M. G., Gunn-Moore, F. J. & Antkowiak, M. All-Optical Assay to Study Biological Neural Networks. *Frontiers in neuroscience* **12**, 451 (2018).

8. Dana H., Guo C., Shields B.C., Chen T.-W., Kerr R.A., Jayaraman V., Looger L.L., Svoboda K., Kim D.S., GCaMP6s Transgenic Mice for Neuronal Activity Imaging *in Vivo*. Poster session presented at: *Neuroscience;* 2013 Nov 9-13; San Diego, CA.

9. Wong, R. Calcium imaging and multielectrode recordings of global patterns of activity in the developing nervous system. *Histochem J* **30**, 217-229 (1998).

10. Stiebler, I., Neulist, R., Fichtel, I. & Ehret, G. The auditory cortex of the house mouse: left-right differences, tonotopic organization and quantitative analysis of frequency representation. *J Comp Physiol*, 559-571 (1997).

11. Guo, W. *et al.* Robustness of cortical topography across fields, laminae, anesthetic states, and neurophysiological signal types. *The Journal of neuroscience* **32**, 9159-9172 (2012).

12. Issa, J. *et al.* Multiscale Optical Ca2+ Imaging of Tonal Organization in Mouse Auditory Cortex. *Neuron (Cambridge, Mass.)* **83**, 944-959 (2014).

13. Tsukano, H. *et al.* Delineation of a frequency-organized region isolated from the mouse primary auditory cortex. *Journal of neurophysiology* **113**, 2900-2920 (2015).

14. Liu, J. *et al.* Parallel Processing of Sound Dynamics across Mouse Auditory Cortex via Spatially Patterned Thalamic Inputs and Distinct Areal Intracortical Circuits. *Cell reports (Cambridge)* **27**, 872-885.e7 (2019).

15. Romero, S. *et al.* Cellular and Widefield Imaging of Sound Frequency Organization in Primary and Higher Order Fields of the Mouse Auditory Cortex. *Cerebral cortex (New York, N.Y. 1991)* **30**, 1603-1622 (2020).

16. Anderson, R., Knight, P. & Merzenich, M. The thalamo- cortical and corticothalamic connections of AI, AII, and the anterior auditory field (AAF) in the cat: evidence for two largely segregated systems of connections. *The Journal of Comparative Neurology* **194**, 664-701 (1980).

17. Reale, R. A. & Imig, T. J. Tonotopic organization in auditory cortex of the cat. *Journal of comparative neurology (1911)* **192**, 265-291 (1980).

18. Merzenich and Brugge 1974

19. Winer, J. A., Miller, L. M., Lee, C. C. & Schreiner, C. E. Auditory thalamocortical transformation: structure and function. *Trends in neurosciences (Regular ed.)* **28**, 255-263 (2005).

20. Hackett, T. A., Barkat, T. R., O'Brien, B. M. J., Hensch, T. K. & Polley, D. B. Linking Topography to Tonotopy in the Mouse Auditory Thalamocortical Circuit. *The Journal of neuroscience* **31**, 2983-2995 (2011).

21. Schreiner, G. K. J. DOVER, Lysias and the Corpus Lysiacum (Sather Classical Lectures, 39). Berkeley and Los Angeles, Univ. of Calif. Pr., 1968. X, 200 p. Pr. sh. 54. *Mnemosyne* **26**, 67-69 (1973).

22. Saenz, M. & Langers, D. R. M. Tonotopic mapping of human auditory cortex. *Hearing research* **307**, 42-52 (2014).

23. Ohga, S. *et al.* Direct Relay Pathways from Lemniscal Auditory Thalamus to Secondary Auditory Field in Mice. *Cerebral cortex (New York, N.Y. 1991)* **28**, 4424-4439 (2018).

24. Tsukano, H. *et al.* Reconsidering Tonotopic Maps in the Auditory Cortex and Lemniscal Auditory Thalamus in Mice. *Frontiers in neural circuits* **11**, 14 (2017).

25. Polley, D. B., Read, H. L., Storace, D. A. & Merzenich, M. M. Multiparametric Auditory Receptive Field Organization Across Five Cortical Fields in the Albino Rat. *Journal of Neurophysiology* **97**, 3621-3638 (2007).

26. Niemczura, A. C. *et al.* Physiological and Behavioral Responses to Vocalization Playback in Mice. *Frontiers in behavioral neuroscience* **14**, 155 (2020).

27. Lahvis, G. P., Alleva, E. & Scattoni, M. L. Translating mouse vocalizations: prosody and frequency modulation. *Genes, brain and behavior* **10**, 4-16 (2011).

28. Moles, A., Costantini, F., Garbugino, L., Zanettini, C. & D'Amato, F. R. Ultrasonic vocalizations emitted during dyadic interactions in female mice: A possible index of sociability? *Behavioural brain research* **182**, 223-230 (2007).

29. Grimsley, J. M. S., Monaghan, J. J. M. & Wenstrup, J. J. Development of Social Vocalizations in Mice. *PLoS ONE* **6** (2011).

30. Honma, Y. *et al.* Auditory Cortical Areas Activated by Slow Frequency-Modulated Sounds in Mice. *PloS one* **8**, e68113 (2013).

31. Ehret, G. & Bernecker, C. Low-frequency sound communication by mouse pups (Mus musculus): wriggling calls release maternal behaviour. *Animal Behaviour* **34**, 821 (1986).

32. Geissler, D. B. & Ehret, G. Auditory perception vs. recognition: representation of complex communication sounds in the mouse auditory cortical fields. *The European journal of neuroscience* **19**, 1027-1040 (2004).

33. Schiavo, J. K. *et al.* Innate and plastic mechanisms for maternal behaviour in auditory cortex. *Nature* **587**, 426 (2020).

34. Binder, J. R. *et al.* Human Temporal Lobe Activation by Speech and Nonspeech Sounds. *Cerebral Cortex* (2000).

35. Levy, R. B. *et al.* Circuit asymmetries underlie functional lateralization in the mouse auditory cortex. *Nat Commun* **10** (2019).

36. Marlin, B. J., Mitre, M., J. A., Chao, M. V. & Froemke, R. C. Oxytocin enables maternal behaviour by balancing cortical inhibition. *Nature (London)* **520**, 499-504 (2015).

37. Gordon K.A., Wong D.D.E., Papsin B.C. Bilateral Input Protects the Cortex from Unilaterally-Driven Reorganization in Children who are Deaf. *Brain* 1609:1625 (2013).

38. Oertel, V. *et al.* Reduced Laterality as a Trait Marker of Schizophrenia--Evidence from Structural and Functional Neuroimaging. *The Journal of neuroscience* **30**, 2289-2299 (2010).

39. Steinmann, S., Leicht, G. & Mulert, C. The interhemispheric miscommunication theory of auditory verbal hallucinations in schizophrenia. *International journal of psychophysiology* **145**, 83-90 (2019).

40. Chen, C., Kanold P.O. Bilateral widefield imaging in mice reveals experience dependent asymmetric functional interhemispheric connectivity between left and right auditory cortices. *Johns Hopkins University Library* (2022).